Temperature sensitivity of OH-lines in the H-band of K-M giants

Kasper Lindqvist

Division of Astrophysics
Department of Physics

LUND
UNIVERSITY

2024–EXA219

Degree project of 15 higher education credits
January 2024

Supervisors: Nils Ryde & Govind Nandakumar

Division of Astrophysics
Department of Physics
Box 118
SE-221 00 Lund
Sweden

Abstract

To properly understand regions of space behind interstellar dust, like the Galactic bulge, infrared (IR) observations are needed, as it passes through the dust with minimal absorption. In the past few decades, the development of IR telescopes has allowed for a much deeper understanding of our Galaxy's stellar populations and history. To properly use the data which these IR telescopes produce however, techniques for finding primary parameters of the observed stars are needed however.

One molecule which has been found to be reliably temperature sensitive in the past has been OH, which fills the H-band (15000Å - 18000Å) with hundreds of absorption lines. It has not been known which of these work the best, as previously existing methods only checked subsets of OH-lines, as well as checking over smaller star samples.

It is the goal of this thesis to find a list of high quality OH-lines which all are sensitive to changes in stellar parameters, so that future researchers may use this list as a basis for finding the parameters of stars. These would include the effective temperature, surface gravity and metallicity.

Using 78000 K-M giant spectra acquired from APOGEE DR17, 68 OH-lines have been found to be temperature sensitive out of a total 186 OH lines. This was found from relating line depth and stellar surface temperature, which showed a linear relation for these 68 OH-lines. These 68 lines also lacked any major blends with other atoms and molecules. In addition, a subset of 20 lines of these 68 were shown to be significantly less scattered than the rest.

Populärvetenskaplig beskrivning

As we look out into our Galaxy with today's telescopes, we notice many types of stars. Some are recognisable with comparable mass, chemical composition and size to our sun. Some are a little stranger with different masses, radii and elemental make-up. Another variable one might even see with ones own eye is color. Warmer stars have a bluer tint and colder stars are redder. This is in fact one of the most fundamental parameters of any star, surface temperature. Knowing the surface temperature of a star can lead a researcher do deduce its age and chemical composition, and with enough stars, this allows them to puzzle together the story of our Galaxy. My project strives to more accurately figure out this surface temperature, allowing future scientists to tell us of the Galaxy's tale, billions of years in the making.

An area of our Galaxy that we still lack a lot of insights on is the galactic bulge, also known as the centre of our Galaxy. The reason for this lack of knowledge is cosmic dust. In the galactic disk, which we are located in, clouds of dust have gathered over billions of years. These clouds absorb and scatter optical light, making many of our previous and current telescopes unable to gather data in any region like the bulge. Luckily, infrared light in the near infrared (NIR) does pass through them with ease making cooler red stars optical behind the clouds for NIR telescopes. These are for example stars like the sun which have grown old, increasing their radii and luminosity considerably and cooling off, resulting in them becoming red giants.

So what can these red giants tell us? Through spectroscopy, the process of splitting light into its constituent colors, known as wavelengths, one can see which wavelengths of light is radiated by these stars. From this spectrum of wavelengths, emission peaks and absorption troughs can be spotted. These are related to elements in the atmosphere of the observed star. For example, a star with a lot of iron would have deep absorption lines where iron atoms are known to absorb light. This holds true for all elements and molecules. By then relating the absorption strength with other intrinsic properties of a star's surface, like surface gravity and surface temperature, one can figure out he chemical make-up of the given star. By then knowing the elements in many stars of the bulge, we get closer to a full understanding of the Milky Way's history.

Not all wavelengths that any given atom or molecule absorbs are created equal however. The absorption lines of the molecule OH for example are generally known to decrease in strength gradually when going from 3000 stars, down to non-existence in stars hotter than 4000. This is due to the molecule breaking down into its con-

stituents the hotter its environment. And though this is generally true, this does not hold for all lines. Some lines are very weak even in the coldest of stars, some lines break the relation totally by being both deep and shallow in similarly cold stars, and some lines do hold to the relation but blend too much with neighboring lines to be useful. Therefore, my goal with this thesis is to figure out which specific lines of the molecule OH are most sensitive and least scattered to temperature. Only a handful of all possible OH-lines in the near infrared have been discovered to be temperature sensitive, but by analysing the line depth of all viable lines, many more lines may be used to calibrate the surface temperature of bulge star temperatures.

Contents

Chapter 1

Introduction

Since the late 1600s with Sir Isaac Newton's description of sun light as composed of the rainbow's colors, the field of spectroscopy has flourished (Fara, 2015). As a star generates energy in its core, it heats up. This process then gives rise to thermal radiation which approximates a black body spectrum (Mavani and Singh, 2022).

Something one does notice in the spectrum of any star is that it is not smooth like a characteristic black body but has peaks and troughs. These are atomic and molecular lines. As the light generated in the core of the star passes through its photosphere, it may be absorbed by an atom and so will give off less radiation in that wavelength. Alternatively, if many atoms close to, or outside the surface become excited, they may radiate outwards toward us, increasing the radiation in that wavelength. All elements and molecules have hundreds of lines and they give the key to properly understand any given star.

From the spectrum of a star, many quantities which define it can be estimated. This is done in several ways. One parameter is effective temperature. A way to find it is by comparing radiation in one wavelength band with another. Another is metallicity. It can be found by analyzing the line strength of absorption lines. The shape of absorption lines also tells details of the star. The higher the gravity in the photosphere, known in the literature as surface gravity or log(g), the more pressure broadening occurs, causing absorption lines to look more Lorentzian. On the other hand, the hotter, turbulent and quickly rotating the photosphere is, absorption lines look more Gaussian. How a star is moving relative to us can also be measured due to the visible shift in the spectrum caused by the Doppler effect.

Knowing these parameters of stars in our and other galaxies is crucial for all kinds of astronomy. Knowing the velocity of stars allows for better mapping of how our universe is currently, and historically looked like. Knowing the metallicity of stars can tell us what types of stars came before our current stars. Surface gravity and rotational velocity both indicate the size of that star, as well how old the star might be. This does require the mass of the star as well however, which shows that other methods outside spectroscopy are needed within astrophysics in general. Finally, effective temperature sets the dynamics of what can actually happen in the photosphere of stars, as well as what processes occur deeper into the star. Together, these parameters join up to give a fuller understanding of how atoms interact, how heavy elements have been formed and how big our universe is.

1.1 Infrared Spectroscopy

One major problem plaguing optical light spectroscopy is the extinction of light by interstellar clouds. This is due to dust scattering optical light very well (Jönsson et al., 2017). A good way to avoid this is by instead looking in the infrared spectrum. Here, light can mostly pass through unabated which allowes for spectroscopic analysis of whatever hides behind. This allows for data analysis of stars within protoplanetary discs and stars behind interstellar dust clouds. It also gives spectroscopic data for cooler objects like dark nebulae and brown dwarfs, as they are not hot enough to transmit in the optical range. In addition, cooler stars like K-types and M-types radiation peak is in the low infrared, allowing telescopes to find more cool stars in the infrared than in the optical.

A problem with infrared spectroscopy which is less problematic in optical is the earth's atmosphere. It is for the most part transparent in the optical range, but mostly opaque in the infrared. Luckily enough, certain wavelength bands do exist where the atmosphere is see-through. The three closest to the optical are the H-band (centered on 1.65μm), K-band (centered on 2.2μm) and L-band (centered on 3.5μm). Out of these, the H-band has been shown to probe deeper into stars photosphere, giving more information of the stellar abundances of observed stars (Wing and Jorgensen, 2003).

1.2 Stellar parameters

To be able to know the history and future of a star, one needs to find characteristics which describe it. Therefore, several parameters have been defined to do just that. Effective temperature, T_{eff}, surface gravity, log(g), metallicity, Fe/H, micro turbulence ν_{micro}, radial velocity, RA, and element specific abundances, element/Fe, are some of the most common parameters when describing stars. Out of these, the effective temperature does set the average energy of particles in the photosphere however, and so can be seen as more important when dealing with molecular abundances and particle interactions within the photosphere.

When talking of effective temperature, it is important to understand what is meant by it. In particular, it is not a uniform temperature at a particular "surface" of the star. This is due to most stars outer layer. Instead of being solid is a turbulent atmosphere of plasma and gas which gets increasingly dense the deeper one goes. The effective temperature then is defined by Stefan–Boltzmann law.

$$\int_0^\infty F_\lambda d\lambda \equiv \sigma T_{eff}^4 \tag{1.1}$$

It states that the flux F_λ over all wavelengths is equal to Boltzmann's constant times the effective temperature to the forth power. (Gray, 2008).

1.3 Temperature estimations

Though effective temperature is a very fundamental value to find from a star, it is not as easy as to put a thermometer in the star and reading of the output. All stars have colder and warmer regions. The sun for example has a effective temperature of 5800, however this does not mean that at a radius defined as the surface, the sun is at a constant 5800. Instead, one uses different methods to relate the light intensity of a star to estimate an effective temperature. Here follows a few major methods used to calculate the effective temperature of stars.

1.3.1 Interferometry

By finding the flux, distance to and radius of a star in the sky, its effective temperature can be found via Boltzmann's law. Interferometry allows for the possibility of the angular width and distance of the star to be calculated. This however is not star agnostic however, as limb darkening can underestimate or overestimate the total

flux of the star, resulting in an error in temperature. As a star needs to be spatially resolved for this to work, only close up stars can be used for this method, however these stars may then be used as benchmark stars to check other methods of deriving T_{eff}(Mozurkewich et al., 2003).

1.3.2 Infrared flux method (IRFM)

When using IRFM, one finds the bolometric flux and an IR monochromatic flux and finds the ratio between them, R_{theo}. This ratio then relates to σT_{eff}^4. Depending on which frequency used to calculate the ratio, different values R_{theo} are known for model atmospheres. This method is best for stars above 4000 due to molecular line absorption below 4000K (Casagrande, 2008).

1.3.3 Spectral synthesis

Using modelling software to synthetically recreate a star, parameters like metallicity and temperature can be set as free variables. These can then iterative change until the difference in synthetic spectrum and observed star spectrum is small. Here, elemental lines known to be sensitive to temperature or metallicity are crucial, as they can become prime locations to compare synthetic and real data.Nandakumar et al. (2023).

1.4 Spectral line formation

As light radiates into the vicinity of an atom's electron cloud, three things could happen. Either the light excites one of the electrons into a more energetic state, or it might pass through without interacting as the electrons lacked any possible energy states which corresponded to that energy, or it could cause induced emission. Molecules like OH has more interacting frequencies than atoms however, as they also get excited into vibrational and rotational states. In a stars spectrum, absorption lines are formed from the first out of the three cases.

When measuring a spectrum of a star, absorption lines appear in the spectrum with different widths and depths. The total absorption or equivalent width in that line is dependent on how much of the photosphere is made up of the particular element/molecule which is the origin of that line, as well as how common this line transition is in the measured star. Effective temperature would therefore have a strong effect on which lines may appear. In a cool star, low-energy transitions would

be common and high-energy transitions non-existent, whilst in a hot star, more of these high-energy transitions show up. How it is spread and by how much depends on a few factors. Surface gravity and effective temperature causes the biggest spread, however if the micro-turbulence or radial velocity is high, it will also play a role in spreading the line. As the temperature and micro-turbulence cause a Gaussian spread from Doppler broadening whilst the surface gravity makes the spread look Lorentzian from pressure broadening, the final shape will be that of a Voigt profile (Gray, 2008).

1.5 APOGEE

The Apache Point Observatory Galactic Evolution Experiment 1 and 2(APOGEE-1 and APOGEE-2) are programs initially started by Sloan Digital Sky Survey III (SDSS-III) to get a wide scale survey of stars in all major star populations in the Milky Way in the H-band. It is made up of three spectrographs, two of which can be found at Apache Point Observatory (APO) in New Mexico, United States, and one in Irénée du Pont Telescope of Las Campanas Observatory (LCO) in Atacama de Chile. Since its commissioning in 2011, it is now in Data Release 17, providing spectra for more than 657,000 stars (Majewski et al., 2017).

1.5.1 Spectral grids

When APOGEE Stellar Parameters and Abundances Pipeline (ASPCAP) first tries to fit parameters to a star spectrum, a subprogram FEREE interpolates the spectrum into a pre-computed synthetic spectrum which is part of one out of six grids. These are GK giant, GK dwarf, M giant, M dwarf, F and BA All pertain to different effective temperatures, surface graveties, metallicities, micro-turbulence and rotational velocities[1]. From this initial fit, ASPCAP finds where in this grid the particular star belongs. What this results in is a data set with clearly demarcated edges, as seen at 3100, 3900 and 0.5 dex in figure 1.1 (Jönsson et al., 2020).

[1] `https://www.sdss4.org/dr17/irspec/apogee-libraries/`

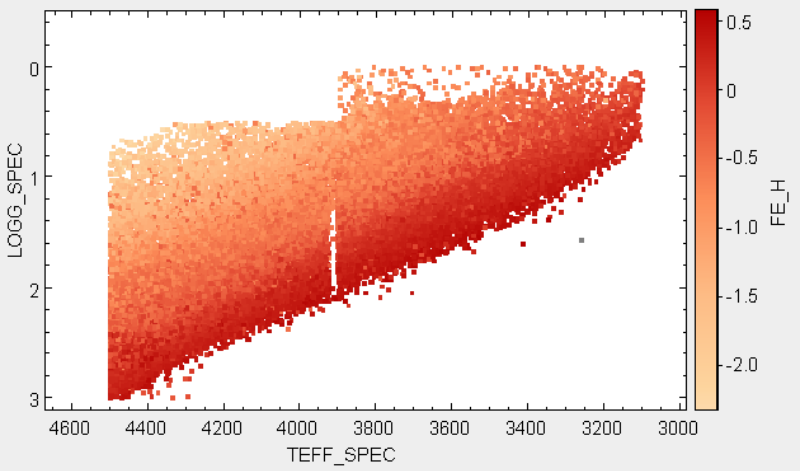

Figure 1.1: All APOGEE stars with surface temperature between 3000 to 4500, surface gravity 0 dex to 3 dex, SNR bigger than 80, and ASPCAP and STAR flags set to zero.

1.5.2 Stellar parameters

Through ASPCAP, most stars in the APOGEE database have an associated effective temperature, surface gravity and metallicity, and many other calibrated values, however these three deserve more time as they are the basis for most other derived parameters of each star.

Effective temperature is determined in two different ways in APOGEE, one called the calibrated T_{eff} which goes under the TEFF tag, and one called the spectroscopically determined T_{eff} which goes under the TEFF_SPEC tag. TEFF_SPEC takes the raw spectroscopic data and fits itself to that, whilst TEFF was calibrated to the photometric scale of (González Hernández and Bonifacio, 2009). This TEFF is calibrated for stars between 4500 to 7000, so _SPEC values should be used under 4500.
Similarly to effective temperature, surface gravity also has a calibrated LOGG and an uncalibrated LOGG_SPEC. Here LOGG_SPEC is found by fitting to the raw spectroscopic data, whilst LOGG comes from a calibration relating APOGEE's spectral data with stars in the Kepler field which contain surface gravity data (Pinsonneault et al., 2018). The calibrated LOGG uses TEFF as part of the calibration.
FE/H is similarly found by ASPCAP by first estimating a value and then via small increases and decreases, it stabilizes around a particular value (Jönsson et al., 2020).

1.5.3 ASPCAP and STAR flags

Many stars lack good data for one reason or another. Some have calculated parameters which seem untrustworthy. These stars get an ASPCAP-flag. This means that if one wants to only use stars with very reliable parameters, one only uses stars with ASPCAPFLAG == 0. STAR-flags on the other hand are set when the spectrum of any given star lacks enough information. This might be when the signal-to-noise ratio (S/N) is below 70, or when more than 20% of pixels in the raw data does not align with the other pixels at all. Similarly to the ASPCAP flags, setting STARFLAG == 0 assures that only good spectra are selected.[2] (Holtzman et al., 2018)

1.5.4 APSTAR and ASPCAP spectra

APOGEE has two different spectra which have their own uses depending on your goal. APSTAR spectra are combined spectra of multiple observations of the same star. This increases S/N, making absorption and emission lines clearly visible with the downside of not having been normalized. This means one needs to find continuums in the spectrum to find line depth or equivalent width relative to other stars. ASPCAP spectra solve the un-normalized part by fitting a spectrum to the ASPCAP parameters created in ASPCAP, creating a pseudo continuum-normalised spectrum. This allows for analysis of APOGEE parameters to see how well they correspond with the manual data. For this project, the APSTAR spectra are therefore the obvious choice of spectra, as it allowes for analysis of actual raw star data.[3]

[2] `https://www.sdss4.org/dr17/irspec/apogee-bitmasks/`
[3] `https://www.sdss4.org/dr17/irspec/spectra/`

Chapter 2

Method

To find the most temperature sensitive OH-lines for K-M giants in the H-band, three things are needed: A robust list of all OH-lines which are not too blended with neighboring lines, a good quality sample of K-M giants with reliable metallicity, surface temperature and surface gravity, and finally a code which can determine the line depth of any given OH-line for any given star. These line depths are then plotted over temperature and split into metallicity bins to see which lines are most temperature sensitive, least noisy, and at which temperatures any given line may be used.

2.1 OH-line sample

A comprehensive list of all known OH-lines in the H-band is collected (Hinkle et al., 2000). To find which of these lines are possibly useful, a high resolution sample star spectrum - $\lambda/\Delta\lambda = 45000$ - produced by IGRINS, a compact high-resolution near-infrared spectrograph at Gemini South, is plotted. For each OH-line it is noted if the line is visible or if it is overlapping with other unknown, or otherwise difficult lines. If it stands alone or only overlaps with a weaker line, it is kept. This selection process can be seen in figure 2.1, where the OH-line on the left is discarded due to some very odd overlapping with other lines, while the right OH-line is kept as it does not seem to overlap with any other elemental or molecular lines.

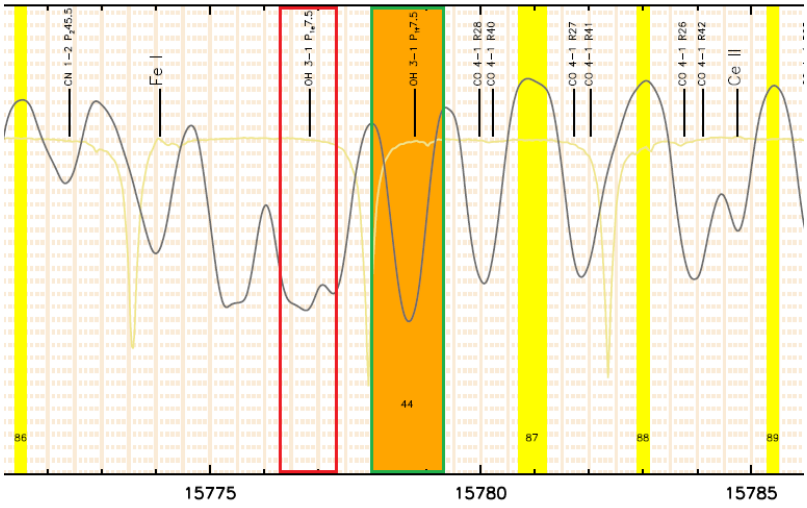

Figure 2.1: Here we see a telluric absorption spectrum in beige and a spectrum of a star (2MASS ID: 2M14240039-6252516) in black marked with four coninuums in yellow and one OH-lines. The left line circled in red is discarded due to it overlapping strongly with other lines, and the right line circled in green which is kept as it does not overlap strongly with another identified OH-line.

2.2 Stellar sample

To get a big enough sample size of stars, APOGEE DR17 is used (Abdurro'uf et al., 2022). This set contains 733901 stars, including main sequence stars and giant stars. A limited set of 78195 stars is taken from the APOGEE data such that only K-M giants lacking ASPCAP or STAR data flags remain. This subset can be seen in figure 1.1. After extracting the APOGEE star names and data for each valid star, the spectrum data for each star is retrieved[1] (Abdurro'uf et al., 2022). From each of these files, a text file is extracted which gives the full H-band spectrum for each star. This intensity over wavelength plot is then used in the line depth calculator.

2.3 Line depth calculations

As none of the APSTAR spectra from APOGEE are normalized, one needs to first estimate a continuum. By analysing the same spectrum which was used to find all

[1] `https://data.sdss.org/sas/dr17/apogee/spectro/redux/dr17/stars/`

viable OH-lines, flat and high-flux regions called continuums are identified surrounding each line, as seen by the yellow continuum regions in figure 2.1. Between these continuums, a linear fit is then made to estimate how the continuum would have looked had there not been any line absorption there. This can be seen as a gray line in figure 2.2. Then, a ratio between the non-normalized line depth intensity and continuum intensity is calculated to give the normalized line depth ratio for that line and star. This non-normalized line depth is seen as a vertical yellow line in figure 2.2.

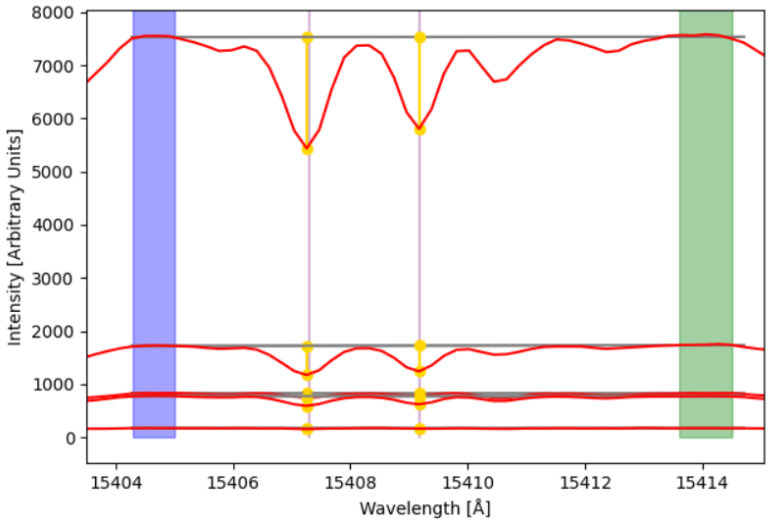

Figure 2.2: Four star spectra plotted over wavelength with two OH-lines at 15407Å and 15409Å. For each spectrum, a continuum is fitted over the two lines by making a linear regression between the continuum masks (in blue and green). From this continuum, a line depth is found from it to the bottom of each line (in yellow). This line depth is then divided by the continuum height go give a value between 0 and 1. This normalized line depth is then compared between stars.

Initially, the plan was to use equivalent width as a measure of line strength, as it would also account for the absorption in the wings of the line. This was found to only reduce the accuracy of the end data however as APOGEE's data set has a resolution much smaller than needed, about 22000. This resulted in much of the data being augmented by neighboring lines. Only taking the line depth of each line will therefore make the lines temperature sensitivity much more reliably found. The reason this simplification can be done is that no lines spread more than APOGEE's resolution. This is in part thanks to the fact that red giants lose a lot of rotational

velocity as they grow older and swell up, putting more mass further from its axis of rotation making them rotate slower.

Chapter 3

Results and Discussion

The following is a presentation of each step performed to find the most temperature sensitive OH lines in the H-band.

3.1 Line pruning

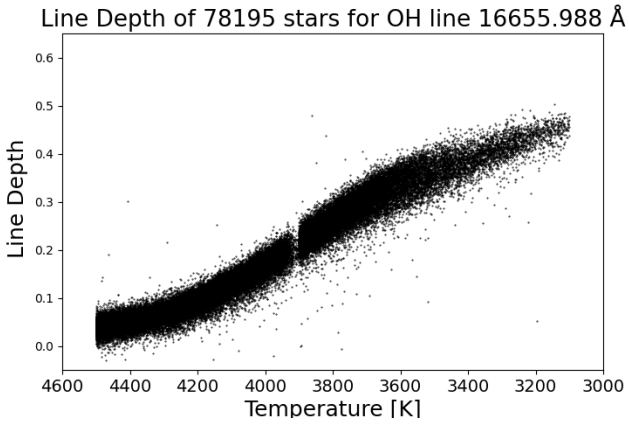

Figure 3.1: OH-Line 16655.988Å with calculated line depth for 78195 K-M giants over their APOGEE estimated TEFF_SPEC temperature.

After a thorough investigation of 186 known OH-lines in the high resolution IGRINS spectrum, 96 OH lines were kept. These lines lacked any major blends. Finding continuums around each OH-line then allowed for the line depth to be calculated for any given line of any given star. For each line, a plot was then created, plotting the

calculated line depth of each star over their APOGEE temperature. A nice example can be seen in figure 3.1. Four other lines with odd behaviours can be seen in figure 3.2.

Looking at the four figures in figure 3.2, we can draw some conclusions and ask some questions. OH line 15145.771 has two regimes, one where the line depth slope approximates 0 and one where it linearly decreases as temperature increases. This splitting needs an explanation. OH line 15897.705Å has a big spread in line depth over the warm range but is very tight in the cool range. If there is no specific reason which determines this spread, as a star with 0.3 line depth at 15897.705Å could be anywhere from 3800 to 4500+ Kelvin. OH line 16346.176 Å is clearly very weakly dependent on temperature as its slope is very shallow. In addition, it is also quite noisy. Therefore it is not a good line to keep. Finally, OH line 16909.284Å also splits, but it instead splits in the cool range into two distinct groups. Like with 15145.771Å, this needs investigation.

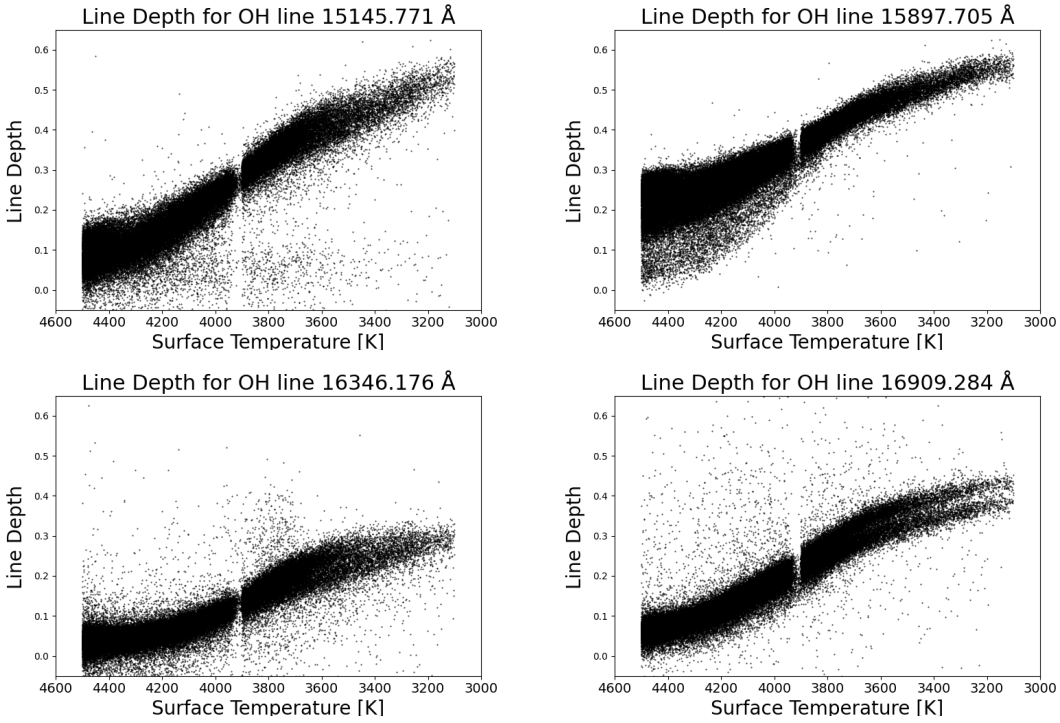

Figure 3.2: Line depth over temperature plot for 78195 stars (top left with 76453 stars due to lacking line depth data for 1742 stars), for four out of 96 selected OH-lines in the H-band.

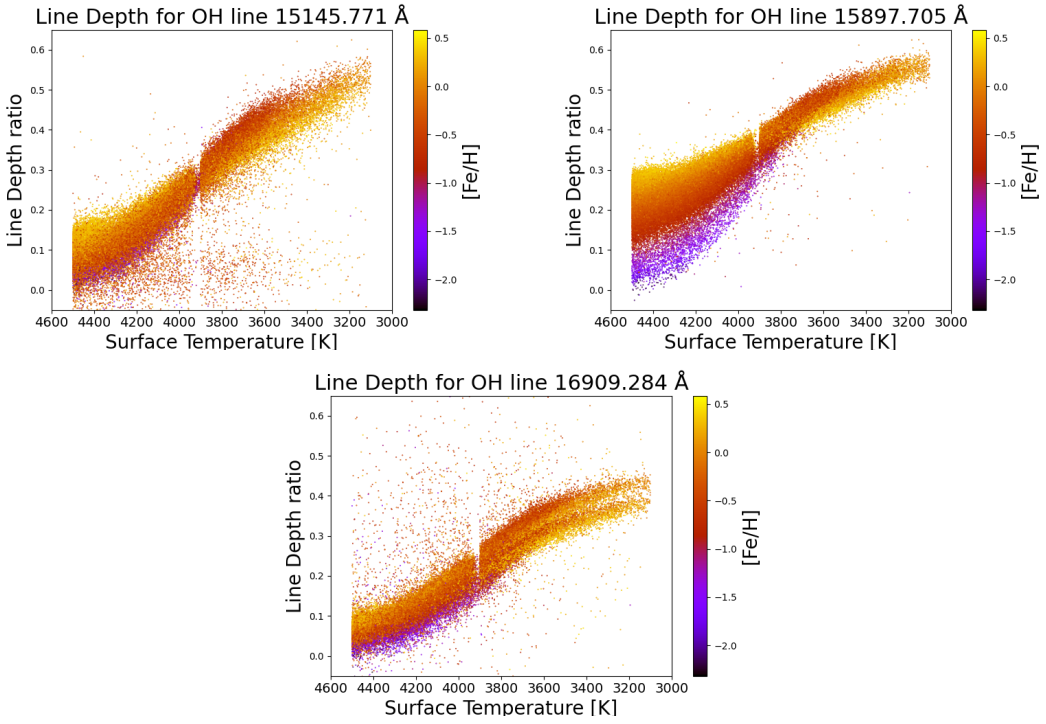

Figure 3.3: Line depth over temperature plot for 78195 stars (top left with 76453 stars due to lacking line depth data for 1742 stars), for three out of 96 selected OH-lines in the H-band, colored by their respective metallicity.

To determine the reason for the splitting, the three remaining unexplained plots were colored by metallicity as seen in figure 3.3. Across all plots, a general trend is seen where line depth increases with metallicity for warmer stars and decreases with metallicity for cooler stars. The reason for this is unknown and needs to be further studied in future papers. One hypothesis would be that for cooler effective temperatures, highly metallic stars contain more carbon, which would cause an increase in CO production and decrease OH production, while for hotter effective temperatures, highly metallic stars contain a higher abundance of oxygen relative to carbon, promoting OH production over CO. 15145.771Å and 16909.284Å are still mysteries, but for different reasons. Line 15897.705Å however has an answer to its spread. For hot stars, this line is highly metallicity dependent, while for cooler stars, its not very metallicity dependent. That is odd, as most lines were not this sensitive at hotter temperatures, and a closer look at the spectra of the stars are needed to properly explain this oddity. 15145.771Å is still a mystery but like with 15897.705Å, looking

at the star spectra might enlighten us to what is happening. As for 16909.284Å, as well as four other OH-lines, 16895.179Å,16898.766Å, 16902.7728Å and 16904.275Å, they all have a similar problem. In specific, they all fork into two distinct regions in the pre-3800 range, each with a low metallicity top and high metallicity bottom. Similar plots were made for log(g), ν_{micro} and O/Fe as color-bars and all of these parameters share this problem. As of now, I have not found a satisfying answer for why it forks, nor why it only does so in the 16890Å-16910Å range. As APOGEE's spectra cut off at 17000Å, we cannot know if this splitting would continue for lines beyond 16910Å either. A deeper analysis of these OH-lines might illuminate the reason for this odd behaviour, perhaps by using spectra of higher resolution.

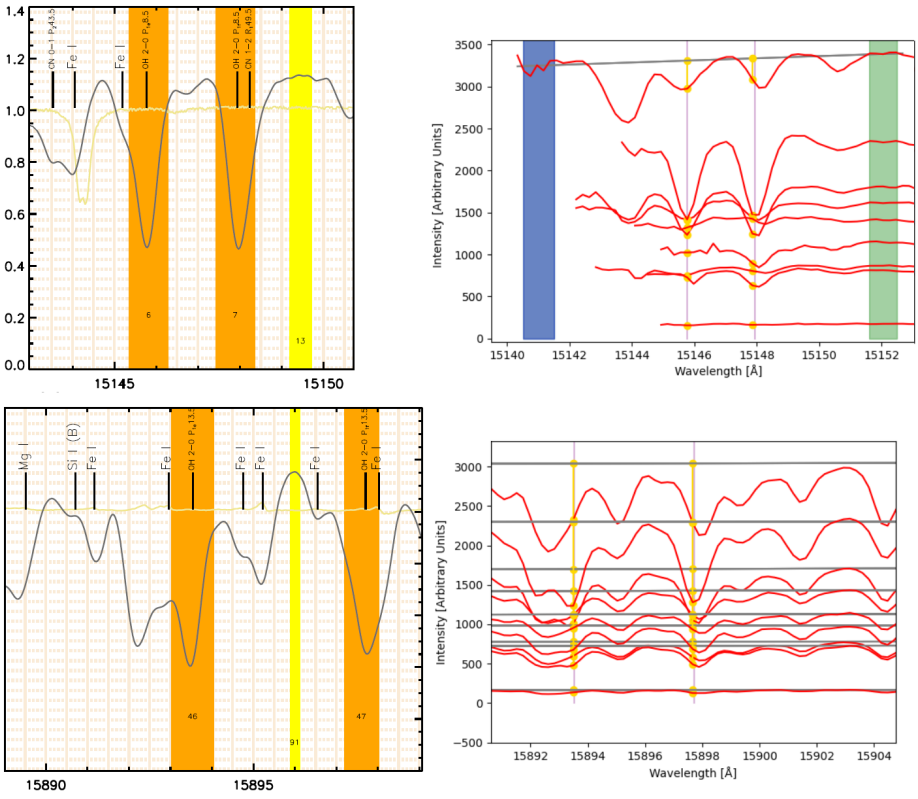

Figure 3.4: Left figures shows an IGRINS spectrum of different wavelength ranges, with OH-lines marked in orange. The right shows two figures with identical ranges to the left figures but which is instead plotting 9 APOGEE spectra, with OH-lines marked with vertical lines.

In figure 3.4, a high resolution IGRINS spectrum is shown on the left, with OH

lines marked with orange, and elemental and molecular lines marked with black lines on top. To the right, the same wavelength range is shown with corresponding OH-lines as those on the left. Here, nine different APOGEE star spectra are plotted. A gray line is fitted between a left continuum and a right continuum.

As seen in figure 3.4, many stars lacked data over the left continuum for line 15145.771Å. This explains why two distinct regions were formed in figure 3.2. One whose left continuum existed and became part of the nice curve, and one whose left continuum was defined as the left most value in its list, which caused the linear continuum fit to go crazy. If this error would have been spotted earlier, 15145.771Å and three other lines, 15129.665Å, 15130.992Å, and 15147.942Å, might have been saved and been part of the final 20 best OH-lines. As it stands, they were in this step omitted from the list of useful lines. In future studies into the temperature sensitivity of OH-lines, it would be fruitful to analyse these and shorter wavelength OH lines, such as 15002.152Å, 15003.120Å, and 15022.868Å.

The OH-line at 15897.705 also is explained using figure 3.4. As seen in the high resolution spectrum, this OH-line is bordering an iron line. In the nine APOGEE spectra plot on the right, it can also be seen that the absorption line looks to be shifted to the right due to this iron line. So, for warm stars, the OH-line is very weak, so as Fe/H increases, the tail of the iron line increases the line depth at 15897.705Å. For cooler stars, this observation does not hold as Fe line strength does not increase nearly as much for any given increase in Fe/H. This OH-line does bring an interesting realization however. Looking at the 4400 - 4500 region, the high metallicity yellow region and low metallicity blue regions look pretty flat, while the middling metallicity red region clearly has a linearly decreasing trend. This implies that how useful any given OH-line will be dependent on the star's metallicity.

All these steps were taken for each of the 96 OH-line still seen as viable. After this was done, 68 OH-lines remained.

3.2 Data shape

To analyze the data gathered, a good way of organizing it is important. In figure 3.5, all 78195 stars with their respective T_{eff}, metallicity and calculated line depth have been plotted in one of eight subplots. Each subplot covers a separate metallicity ranges, -2.5 to -1.25 dex, -1.25 to -1.0 dex, -1.0 to -0.75 dex, -0.75 to -0.5 dex, -0.5

to 0.0 dex, 0.0 to 0.25 dex, and 0.25 dex to 0.6 dex. To find at what temperature any given OH-line has a slope big enough to qualify as usable, seven linear fits was made to span from 3100 to 4500, meaning that each linear fit spanned a 200K range. If this slope was shallower than $-2 \cdot 10^{-4}$ 1/K, that OH-line was not considered temperature-sensitive enough in that temperature and metallicity range. If however the slope was steeper than the set limit of $-2 \cdot 10^{-4}$ 1/K, the line was considered to be temperature-sensitive in that particular temperature and metallicity range. Surrounding all significant slopes in figure 3.5, two purple lines have been plotted. A table was then created to list the average slope, scatter and temperature ranges dependent on metallicity. This list was then shortened to the 20 least scattered plots. In addition to finding the significant temperature ranges, a scatter parameter was calculated to quantify which OH-lines were least noisy. This was done by calculating the standard deviation of the data from the linear fits and then averaging over all bins and metallicity ranges to get a holistic scatter parameter. This scatter parameter ranged from 0.015 to 0.21, and so to limit the number of lines considered good, an upper limit of 0.025 was set. Finally, the average slope was also calculated.

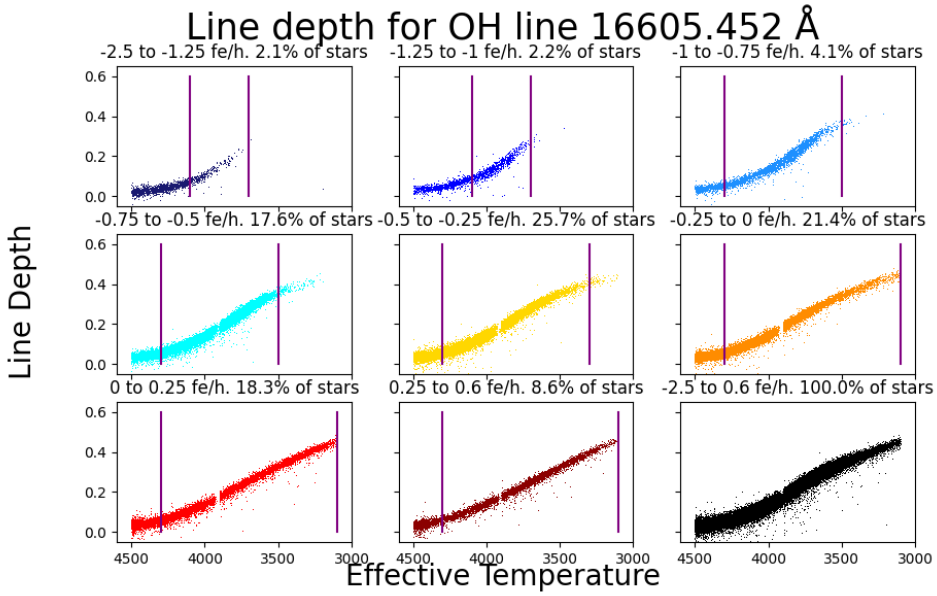

Figure 3.5: Example line $\lambda = 16605.452$Å of line depth data plotted for over temperature and separated into 8 metallicity bins, including a 9'th plot with all stars. Purple lines demarcate the regions where the slope is steep enough to be useful.

3.3 Good and bad OH-lines

In figure 3.6, two out of the 68 lines from section 3.1 are plotted like figure 3.5, with identical metallicity ranges. OH-line 16260.155Å average slope and scatter of -3.337e-4 and 0.0208 while OH-line 16886.269Å has an average slope and scatter of -2.116e-4 and 0.1134 respectively. 16260.155Å has about one fifth the scatter of 16886.269Å and almost a 60% bigger average slope. The slope can be clearly seen in the combined line depth in the black subplots, however the fact that there is a factor 5 difference in the scatter is not so apparent. After thorough observation of the colored metallicity subplots however, one can see more spread in 16886.269Å. From figure 3.6, it is clear that 16886.269Å could probably also be used in a list of OH-lines to find new stars effective temperatures, however as there are many lines with less scatter, 16886.269Å was discarded as to noisy.

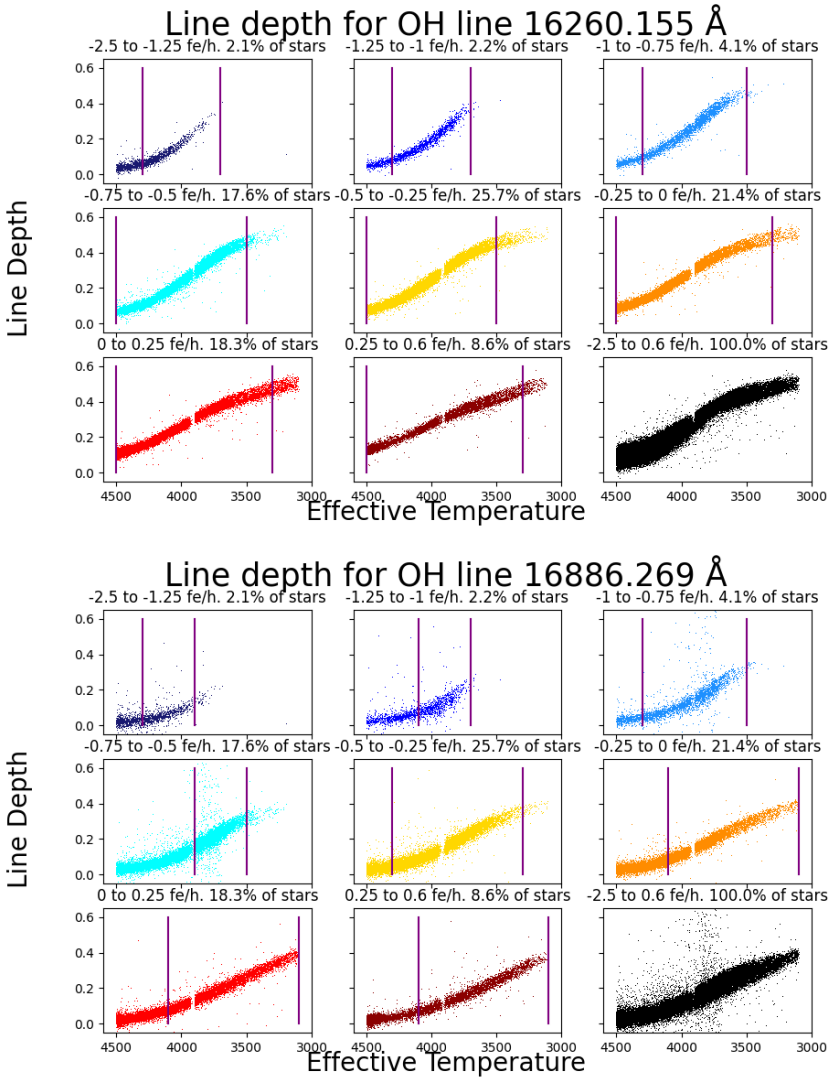

Figure 3.6: Two OH-lines, plotted in the same manner as figure 3.5, displaying a subtle difference in scatter and slope.

3.4 20 best OH-lines

The following is a table (table 3.1) which presents in detail all ranges which each of the 20 least scattered lines are appropriately useful for:

λ	Slope	Scatter	-2.5–1.25 dex	-1.25–1 dex	-1–0.75 dex	-0.75–0.5 dex	-0.5–0.25 dex	-0.25-0 dex	0-0.25 dex	0.25-0.6 dex
[Ångström]	[1/10^4K]	[1/100]	[K]	[K]	[K]	[K]	[K]	[K]	[K]	[K]
15407.292	-4.090	2.422	3700 - 4300	3700 - 4300	3500 - 4500	3500 - 4500	3300 - 4500	3100 - 4500	3100 - 4500	3100 - 4500
15568.785	-3.744	2.360	3700 - 4300	3700 - 4300	3500 - 4300	3300 - 4500	3300 - 4500	3100 - 4500	3100 - 4500	3100 - 4300
15572.088	-3.626	2.392	3700 - 4300	3700 - 4300	3500 - 4300	3500 - 4500	3300 - 4500	3300 - 4500	3100 - 4500	3100 - 4300
15730.444	-3.537	2.122	3700 - 4300	3700 - 4300	3500 - 4300	3500 - 4300	3100 - 4500	3300 - 4300	3100 - 4300	3100 - 4300
15755.520	-3.058	2.093	3700 - 4300	3700 - 4300	3500 - 4300	3500 - 4300	3300 - 4300	3300 - 4300	3300 - 4300	3300 - 4300
15756.528	-2.918	1.846	3700 - 4300	3700 - 4300	3500 - 4300	3500 - 4300	3300 - 4300	3300 - 4300	3300 - 4300	3300 - 4300
15893.537	-3.449	1.928	3700 - 4500	3700 - 4500	3500 - 4500	3500 - 4500	3500 - 4500	3300 - 4500	3300 - 4500	3100 - 4500
15897.705	-3.095	1.973	3700 - 4300	3700 - 4500	3500 - 4300	3500 - 4500	3500 - 4300	3300 - 4300	3300 - 4300	3300 - 4100
15910.418	-2.535	1.969	3700 - 4300	3700 - 4300	3500 - 4300	3500 - 4300	3700 - 4300	3700 - 4300	3900 - 4300	3100 - 4500
15912.728	-2.468	1.966	3700 - 4300	3700 - 4300	3500 - 4300	3500 - 4300	3700 - 4300	3700 - 4300	3100 - 4500	3100 - 4500
16052.765	-3.337	2.306	3700 - 4300	3700 - 4300	3500 - 4300	3500 - 4300	3300 - 4300	3300 - 4300	3100 - 4300	3100 - 4300
16251.663	-3.367	2.487	3700 - 4300	3700 - 4300	3500 - 4300	3500 - 4300	3300 - 4300	3300 - 4300	3300 - 4300	3100 - 4300
16255.018	-3.735	2.361	3700 - 4300	3700 - 4300	3500 - 4300	3500 - 4300	3300 - 4300	3100 - 4300	3100 - 4300	3100 - 4300
16260.155	-3.337	2.081	3700 - 4300	3700 - 4300	3500 - 4300	3500 - 4500	3500 - 4500	3300 - 4500	3300 - 4500	3300 - 4500
16523.502	-3.328	2.361	3700 - 4300	3700 - 4300	3500 - 4300	3500 - 4300	3300 - 4300	3100 - 4300	3100 - 4300	3100 - 4500
16605.452	-3.045	1.558	3700 - 4100	3700 - 4100	3500 - 4300	3500 - 4300	3300 - 4300	3100 - 4300	3100 - 4300	3100 - 4300
16649.949	-3.266	1.858	3700 - 4300	3700 - 4300	3500 - 4300	3500 - 4300	3300 - 4300	3300 - 4300	3300 - 4300	3100 - 4300
16655.988	-3.282	1.817	3700 - 4300	3700 - 4300	3500 - 4300	3500 - 4300	3300 - 4300	3100 - 4300	3100 - 4300	3100 - 4300
16662.201	-2.860	1.864	3700 - 4300	3700 - 4300	3500 - 4300	3500 - 4300	3300 - 4300	3300 - 4300	3300 - 4300	3300 - 4100
16729.779	-2.788	2.346	3700 - 4100	3700 - 4300	3500 - 4300	3300 - 4300	3300 - 4300	3100 - 4300	3100 - 4100	3100 - 4100

Table 3.1: Here, the 20 least scattered OH-lines are listed with associated temperature ranges depending on metallicity. An average slope is given, as well as the average scatter which tells how thin the data is. Plots of all lines can be seen in Appendix B

Chapter 4

Conclusion

The overarching goal of this thesis was to find which OH-lines would be most appropriate to use when determining parameters of unknown K-M giants.
It was found that equivalent width would not work for this thesis as a measure of line strength as APOGEE's lower spectral resolution would include severe close-by blends. This in turn would bring neighbouring lines into the integration limits, scattering the data.
What did give reliable data of which lines were sensitive or not was line depth. In addition, metallicity was also found to be of strong influence based on detailed analysis by color coding the line depth versus temperature relation with metallicity for each line.
Using APOGEE data did come with a bit of problems. Firstly, it lacked data for lines outside 15180Å to 17000Å, cutting out 73 possibly great OH-lines. Secondly, as it forced us to use line depth instead of equivalent width, the data might have preferentially treated lines which deepened more than they broadened, discarding OH-lines which could have worked in higher resolution stars.
20 lines were found which all show less scatter than previously used OH-lines however. Therefore, future studies into stellar parameter estimation will hopefully be able to use these lines to more accurately deduce stellar parameters of K-M giants [Kocher et al. (in prep.)].

Bibliography

Abdurro'uf, N., Accetta, K., Aerts, C., Silva Aguirre, V., Ahumada, R., Ajgaonkar, N., Filiz Ak, N., Alam, S., Allende Prieto, C., Almeida, A., Anders, F., Anderson, S. F., Andrews, B. H., Anguiano, B., Aquino-Ortíz, E., Aragón-Salamanca, A., Argudo-Fernández, M., Ata, M., Aubert, M., Avila-Reese, V., Badenes, C., Barbá, R. H., Barger, K., Barrera-Ballesteros, J. K., Beaton, R. L., Beers, T. C., Belfiore, F., Bender, C. F., Bernardi, M., Bershady, M. A., Beutler, F., Bidin, C. M., Bird, J. C., Bizyaev, D., Blanc, G. A., Blanton, M. R., Boardman, N. F., Bolton, A. S., Boquien, M., Borissova, J., Bovy, J., Brandt, W. N., Brown, J., Brownstein, J. R., Brusa, M., Buchner, J., Bundy, K., Burchett, J. N., Bureau, M., Burgasser, A., Cabang, T. K., Campbell, S., Cappellari, M., Carlberg, J. K., Wanderley, F. C., Carrera, R., Cash, J., Chen, Y.-P., Chen, W.-H., Cherinka, B., Chiappini, C., Choi, P. D., Chojnowski, S. D., Chung, H., Clerc, N., Cohen, R. E., Comerford, J. M., Comparat, J., da Costa, L., Covey, K., Crane, J. D., Cruz-Gonzalez, I., Culhane, C., Cunha, K., Dai, Y. S., Damke, G., Darling, J., Davidson Jr., J. W., Davies, R., Dawson, K., De Lee, N., Diamond-Stanic, A. M., Cano-Díaz, M., Sánchez, H. D., Donor, J., Duckworth, C., Dwelly, T., Eisenstein, D. J., Elsworth, Y. P., Emsellem, E., Eracleous, M., Escoffier, S., Fan, X., Farr, E., Feng, S., Fernández-Trincado, J. G., Feuillet, D., Filipp, A., Fillingham, S. P., Frinchaboy, P. M., Fromenteau, S., Galbany, L., García, R. A., García-Hernández, D. A., Ge, J., Geisler, D., Gelfand, J., Géron, T., Gibson, B. J., Goddy, J., Godoy-Rivera, D., Grabowski, K., Green, P. J., Greener, M., Grier, C. J., Griffith, E., Guo, H., Guy, J., Hadjara, M., Harding, P., Hasselquist, S., Hayes, C. R., Hearty, F., Hernández, J., Hill, L., Hogg, D. W., Holtzman, J. A., Horta, D., Hsieh, B.-C., Hsu, C.-H., Hsu, Y.-H., Huber, D., Huertas-Company, M., Hutchinson, B., Hwang, H. S., Ibarra-Medel, H. J., Chitham, J. I., Ilha, G. S., Imig, J., Jaekle, W., Jayasinghe, T., Ji, X., Johnson, J. A., Jones, A., Jönsson, H., Katkov, I., Khalatyan, D. A., Kinemuchi, K., Kisku, S., Knapen, J. H., Kneib, J.-P., Kollmeier, J. A., Kong, M., Kounkel, M., Kreckel, K., Krishnarao, D., Lacerna, I., Lane, R. R., Langgin, R., Lavender, R., Law, D. R., Lazarz, D., Leung, H. W., Leung, H.-H., Lewis, H. M., Li, C., Li, R., Lian,

J., Liang, F.-H., Lin, L., Lin, Y.-T., Lin, S., Lintott, C., Long, D., Longa-Peña, P., López-Cobá, C., Lu, S., Lundgren, B. F., Luo, Y., Mackereth, J. T., de la Macorra, A., Mahadevan, S., Majewski, S. R., Manchado, A., Mandeville, T., Maraston, C., Margalef-Bentabol, B., Masseron, T., Masters, K. L., Mathur, S., McDermid, R. M., Mckay, M., Merloni, A., Merrifield, M., Meszaros, S., Miglio, A., Di Mille, F., Minniti, D., Minsley, R., Monachesi, A., Moon, J., Mosser, B., Mulchaey, J., Muna, D., Muñoz, R. R., Myers, A. D., Myers, N., Nadathur, S., Nair, P., Nandra, K., Neumann, J., Newman, J. A., Nidever, D. L., Nikakhtar, F., Nitschelm, C., O'Connell, J. E., Garma-Oehmichen, L., Luan Souza de Oliveira, G., Olney, R., Oravetz, D., Ortigoza-Urdaneta, M., Osorio, Y., Otter, J., Pace, Z. J., Padilla, N., Pan, K., Pan, H.-A., Parikh, T., Parker, J., Peirani, S., Peña Ramírez, K., Penny, S., Percival, W. J., Perez-Fournon, I., Pinsonneault, M., Poidevin, F., Poovelil, V. J., Price-Whelan, A. M., Bárbara de Andrade Queiroz, A., Raddick, M. J., Ray, A., Rembold, S. B., Riddle, N., Riffel, R. A., Riffel, R., Rix, H.-W., Robin, A. C., Rodríguez-Puebla, A., Roman-Lopes, A., Román-Zúñiga, C., Rose, B., Ross, A. J., Rossi, G., Rubin, K. R., Salvato, M., Sánchez, S. F., Sánchez-Gallego, J. R., Sanderson, R., Santana Rojas, F. A., Sarceno, E., Sarmiento, R., Sayres, C., Sazonova, E., Schaefer, A. L., Schiavon, R., Schlegel, D. J., Schneider, D. P., Schultheis, M., Schwope, A., Serenelli, A., Serna, J., Shao, Z., Shapiro, G., Sharma, A., Shen, Y., Shetrone, M., Shu, Y., Simon, J. D., Skrutskie, M. F., Smethurst, R., Smith, V., Sobeck, J., Spoo, T., Sprague, D., Stark, D. V., Stassun, K. G., Steinmetz, M., Stello, D., Stone-Martinez, A., Storchi-Bergmann, T., Stringfellow, G. S., Stutz, A., Su, Y.-C., Taghizadeh-Popp, M., Talbot, M. S., Tayar, J., Telles, E., Teske, J., Thakar, A., Theissen, C., Tkachenko, A., Thomas, D., Tojeiro, R., Hernandez Toledo, H., Troup, N. W., Trump, J. R., Trussler, J., Turner, J., Tuttle, S., Unda-Sanzana, E., Vázquez-Mata, J. A., Valentini, M., Valenzuela, O., Vargas-González, J., Vargas-Magaña, M., Alfaro, P. V., Villanova, S., Vincenzo, F., Wake, D., Warfield, J. T., Washington, J. D., Weaver, B. A., Weijmans, A.-M., Weinberg, D. H., Weiss, A., Westfall, K. B., Wild, V., Wilde, M. C., Wilson, J. C., Wilson, R. F., Wilson, M., Wolf, J., Wood-Vasey, W. M., Yan, R., Zamora, O., Zasowski, G., Zhang, K., Zhao, C., Zheng, Z., Zheng, Z., and Zhu, K. (2022). The seventeenth data release of the sloan digital sky surveys: Complete release of manga, mastar, and apogee-2 data. *The Astrophysical Journal. Supplement Series*, 259(2).

Casagrande, L. (2008). Infrared flux method and colour calibrations. *Physica Scripta*, 2008(T133):014020.

Fara, P. (2015). Newton shows the light: a commentary on newton (1672) 'a letter

... containing his new theory about light and colours...'. *Philosophical Transactions of the Royal Society A: Mathematical, Physical and Engineering Sciences*, 373(2039):20140213.

González Hernández, J. I. and Bonifacio, P. (2009). A new implementation of the infrared flux method using the 2mass catalogue*. *AA*, 497(2):497–509.

Gray, D. F. (2008). *The Observation and Analysis of Stellar Photospheres*.

Hinkle, K., Wallace, L., Harmer, D., Ayres, T., and Valenti, J. (2000). High Resolution IR, Visible, and UV Spectroscopy of the Sun and Arcturus. In *IAU Joint Discussion*, volume 24 of *IAU Joint Discussion*, page 26.

Holtzman, J. A., Hasselquist, S., Shetrone, M., Cunha, K., Prieto, C. A., Anguiano, B., Bizyaev, D., Bovy, J., Casey, A., Edvardsson, B., Johnson, J. A., Jönsson, H., Meszaros, S., Smith, V. V., Sobeck, J., Zamora, O., Chojnowski, S. D., Fernandez-Trincado, J., Hernandez, A. G., Majewski, S. R., Pinsonneault, M., Souto, D., Stringfellow, G. S., Tayar, J., Troup, N., and Zasowski, G. (2018). Apogee data releases 13 and 14: Data and analysis. *The Astronomical Journal*, 156(3):125.

Jönsson, H., Holtzman, J. A., Allende Prieto, C., Cunha, K., García-Hernández, D. A., Hasselquist, S., Masseron, T., Osorio, Y., Shetrone, M., Smith, V., Stringfellow, G. S., Bizyaev, D., Edvardsson, B., Majewski, S. R., Mészáros, S., Souto, D., Zamora, O., Beaton, R. L., Bovy, J., Donor, J., Pinsonneault, M. H., Poovelil, V. J., and Sobeck, J. (2020). APOGEE Data and Spectral Analysis from SDSS Data Release 16: Seven Years of Observations Including First Results from APOGEE-South. *AJ*, 160(3):120.

Jönsson, H., Ryde, N., Nordlander, T., Pehlivan Rhodin, A., Hartman, H., Jönsson, P., and Eriksson, K. (2017). Abundances of disk and bulge giants from high-resolution optical spectra. I. O, Mg, Ca, and Ti in the solar neighborhood and Kepler field samples. *A&A*, 598:A100.

Majewski, S. R., Schiavon, R. P., Frinchaboy, P. M., Allende Prieto, C., Barkhouser, R., Bizyaev, D., Blank, B., Brunner, S., Burton, A., Carrera, R., Chojnowski, S. D., Cunha, K., Epstein, C., Fitzgerald, G., García Pérez, A. E., Hearty, F. R., Henderson, C., Holtzman, J. A., Johnson, J. A., Lam, C. R., Lawler, J. E., Maseman, P., Mészáros, S., Nelson, M., Nguyen, D. C., Nidever, D. L., Pinsonneault, M., Shetrone, M., Smee, S., Smith, V. V., Stolberg, T., Skrutskie, M. F., Walker, E., Wilson, J. C., Zasowski, G., Anders, F., Basu, S., Beland, S., Blanton, M. R., Bovy, J., Brownstein, J. R., Carlberg, J., Chaplin, W., Chiappini, C., Eisenstein,

D. J., Elsworth, Y., Feuillet, D., Fleming, S. W., Galbraith-Frew, J., García, R. A., García-Hernández, D. A., Gillespie, B. A., Girardi, L., Gunn, J. E., Hasselquist, S., Hayden, M. R., Hekker, S., Ivans, I., Kinemuchi, K., Klaene, M., Mahadevan, S., Mathur, S., Mosser, B., Muna, D., Munn, J. A., Nichol, R. C., O'Connell, R. W., Parejko, J. K., Robin, A. C., Rocha-Pinto, H., Schultheis, M., Serenelli, A. M., Shane, N., Silva Aguirre, V., Sobeck, J. S., Thompson, B., Troup, N. W., Weinberg, D. H., and Zamora, O. (2017). The Apache Point Observatory Galactic Evolution Experiment (APOGEE). *AJ*, 154(3):94.

Mavani, H. and Singh, N. (2022). A concise history of the black-body radiation problem.

Mozurkewich, D., Armstrong, J. T., Hindsley, R. B., Quirrenbach, A., Hummel, C. A., Hutter, D. J., Johnston, K. J., Hajian, A. R., II, N. M. E., Buscher, D. F., and Simon, R. S. (2003). Angular diameters of stars from the mark iii optical interferometer. *The Astronomical Journal*, 126(5):2502.

Nandakumar, G., Ryde, N., Casagrande, L., and Mace, G. (2023). M giants with igrins: I. stellar parameters and -abundance trends of the solar neighborhood population. *Astronomy amp; Astrophysics*, 675:A23.

Pinsonneault, M. H., Elsworth, Y. P., Tayar, J., Serenelli, A., Stello, D., Zinn, J., Mathur, S., García, R. A., Johnson, J. A., Hekker, S., Huber, D., Kallinger, T., Mészáros, S., Mosser, B., Stassun, K., Girardi, L., Rodrigues, T. S., Aguirre, V. S., An, D., Basu, S., Chaplin, W. J., Corsaro, E., Cunha, K., García-Hernández, D. A., Holtzman, J., Jönsson, H., Shetrone, M., Smith, V. V., Sobeck, J. S., Stringfellow, G. S., Zamora, O., Beers, T. C., Fernández-Trincado, J. G., Frinchaboy, P. M., Hearty, F. R., and Nitschelm, C. (2018). The second apokasc catalog: The empirical approach. *The Astrophysical Journal Supplement Series*, 239(2):32.

Wing, R. F. and Jorgensen, U. G. (2003). Stellar Spectra in the H Band. , 31(2):110–120.

Appendix A

The following is 48 OH-lines which did have their temperature ranges calculated, however due to having and above 0.03 scatter, where not added to table 3.1:

λ	Slope	Scatter	-2.5–1.25 dex	-1.25–1 dex	-1–0.75 dex	-0.75–0.5 dex	-0.5–0.25 dex	-0.25-0 dex	0-0.25 dex	0.25-0.6 dex
[Ångström]	[1/10^4K]	[1/100]	[K]	[K]	[K]	[K]	[K]	[K]	[K]	[K]
15182.985	-2.814	5.901	3700 - 4100	3700 - 4100	3500 - 4100	3300 - 4100	3100 - 4100	3100 - 4100	3100 - 3900	3100 - 3900
15236.787	-3.383	17.55	3700 - 4500	3700 - 4100	3500 - 4100	3300 - 4100	3100 - 4300	3100 - 4100	3100 - 4100	3100 - 3900
15264.608	-3.452	3.046	3700 - 4300	3700 - 4300	3500 - 4500	3500 - 4500	3100 - 4500	3100 - 4500	3100 - 4500	3100 - 4500
15266.172	-3.844	4.421	3700 - 4300	3700 - 4300	3500 - 4300	3300 - 4300	3300 - 4300	3100 - 4300	3100 - 4500	3100 - 4500
15278.528	-3.910	5.292	3700 - 4500	3700 - 4500	3500 - 4300	3300 - 4500	3300 - 4500	3100 - 4500	3100 - 4300	3100 - 4300
15281.057	-3.741	5.494	3700 - 4500	3700 - 4300	3500 - 4300	3300 - 4500	3100 - 4500	3100 - 4500	3100 - 4300	3100 - 4300
15391.126	-3.431	5.914	3700 - 4300	3700 - 4300	3500 - 4300	3500 - 4300	3500 - 4300	3500 - 4300	3300 - 4300	3300 - 4300
15419.464	-3.451	10.38	3900 - 4500	3700 - 4300	3500 - 4300	3500 - 4500	3300 - 4500	3300 - 4500	3100 - 4300	3300 - 4300
15422.371	-3.421	7.308	3700 - 4500	3700 - 4500	3500 - 4300	3300 - 4300	3300 - 4300	3100 - 4300	3300 - 4300	3100 - 4300
15427.480	-3.064	9.960	3700 - 4300	3700 - 4100	3500 - 4300	3300 - 4300	3300 - 4300	3500 - 4300	3300 - 4300	3300 - 4500
15428.397	-2.874	10.17	3700 - 4100	3700 - 4100	3500 - 4300	3500 - 4300	3100 - 4300	3100 - 4300	3100 - 4300	3100 - 3900
15505.530	-4.302	3.241	3700 - 4300	3700 - 4300	3500 - 4300	3500 - 4300	3300 - 4300	3300 - 4300	3300 - 4300	3300 - 4300
15535.461	-3.004	5.463	3700 - 4300	3700 - 4300	3500 - 4300	3500 - 4300	3300 - 4300	3300 - 4300	3300 - 4300	3300 - 4300
15626.702	-3.949	4.449	3700 - 4300	3700 - 4300	3500 - 4300	3300 - 4500	3300 - 4300	3300 - 4300	3100 - 4300	3100 - 4500
15627.407	-3.807	4.611	3700 - 4300	3700 - 4300	3500 - 4300	3500 - 4300	3100 - 4300	3100 - 4300	3100 - 4300	3100 - 4500
15651.894	-3.010	7.925	3700 - 4300	3700 - 4300	3700 - 4300	3500 - 4300	3500 - 4300	3100 - 4300	3100 - 4300	3100 - 4100
15653.477	-3.439	6.773	3700 - 4300	3700 - 4300	3500 - 4300	3500 - 4300	3300 - 4300	3100 - 4300	3100 - 4300	3100 - 4100
15717.124	-3.403	2.646	3700 - 4300	3700 - 4300	3500 - 4300	3500 - 4500	3300 - 4500	3100 - 4500	3100 - 4300	3100 - 4300
15719.700	-3.629	2.549	3700 - 4300	3700 - 4300	3500 - 4300	3500 - 4300	3300 - 4300	3100 - 4300	3100 - 4300	3100 - 4300
15778.786	-3.050	2.897	3700 - 4300	3700 - 4300	3500 - 4300	3500 - 4500	3500 - 4500	3500 - 4500	3300 - 4500	3100 - 4500
15910.418	-2.535	1.969	3700 - 4300	3700 - 4300	3500 - 4300	3500 - 4300	3700 - 4300	3700 - 4300	3900 - 4300	Too Shallow
15912.728	-2.468	1.966	3700 - 4300	3700 - 4300	3500 - 4300	3500 - 4300	3700 - 4300	3700 - 4300	Too Shallow	Too Shallow
16036.887	-3.118	5.757	3700 - 4300	3700 - 4300	3700 - 4500	3500 - 4500	3500 - 4500	3500 - 4500	3300 - 4500	3100 - 4500
16038.533	-3.112	4.084	3700 - 4300	3700 - 4300	3500 - 4300	3500 - 4500	3500 - 4500	3300 - 4500	3300 - 4300	3300 - 4500

Table 4.1: OH-lines 15182.985Å to 16038.533Å with average scatter bigger than 0.03

λ	Slope	Scatter	-2.5–1.25 dex	-1.25–1 dex	-1–0.75 dex	-0.75–0.5 dex	-0.5–0.25 dex	-0.25-0 dex	0-0.25 dex	0.25-0.6 dex
[Ångström]	[1/10^4K]	[1/100]	[K]	[K]	[K]	[K]	[K]	[K]	[K]	[K]
16052.765	-3.337	2.306	3700 - 4300	3700 - 4300	3500 - 4300	3500 - 4300	3300 - 4300	3300 - 4300	3100 - 4300	3100 - 4300
16061.704	-3.376	5.748	3700 - 4300	3700 - 4300	3500 - 4500	3500 - 4500	3300 - 4500	3300 - 4500	3300 - 4500	3300 - 4500
16065.059	-3.635	4.927	3700 - 4300	3700 - 4300	3500 - 4300	3500 - 4300	3300 - 4300	3100 - 4300	3100 - 4300	3100 - 4500
16069.526	-3.781	4.393	3700 - 4300	3700 - 4300	3500 - 4300	3500 - 4500	3300 - 4500	3300 - 4500	3100 - 4500	3300 - 4500
16074.164	-3.226	5.175	3700 - 4300	3700 - 4300	3500 - 4300	3500 - 4500	3500 - 4500	3300 - 4500	3300 - 4300	3300 - 4300
16190.132	-3.186	5.165	3700 - 4500	3700 - 4300	3500 - 4300	3500 - 4500	3500 - 4500	3500 - 4500	3700 - 4500	3300 - 4500
16192.125	-2.657	3.978	3700 - 4300	3700 - 4300	3500 - 4500	3500 - 4300	3500 - 4500	3300 - 4500	3700 - 4500	3300 - 4500
16247.886	-3.588	3.145	3700 - 4300	3700 - 4300	3500 - 4300	3500 - 4300	3300 - 4300	3100 - 4300	3100 - 4300	3100 - 4300
16312.702	-3.369	2.908	3700 - 4300	3700 - 4300	3500 - 4300	3500 - 4300	3300 - 4300	3300 - 4300	3100 - 4100	3100 - 4100
16352.218	-3.186	3.857	3700 - 4300	3700 - 4300	3500 - 4300	3500 - 4500	3500 - 4500	3300 - 4500	3300 - 4500	3300 - 4500
16354.575	-2.997	3.446	3700 - 4300	3700 - 4300	3500 - 4300	3500 - 4300	3500 - 4300	3300 - 4300	3500 - 4300	3300 - 4500
16368.132	-3.515	3.543	3700 - 4300	3700 - 4300	3500 - 4300	3500 - 4300	3500 - 4300	3300 - 4300	3300 - 4300	3300 - 4300
16526.242	-3.449	2.543	3700 - 4300	3700 - 4300	3500 - 4300	3500 - 4300	3300 - 4300	3100 - 4300	3100 - 4300	3100 - 4300
16534.578	-3.243	3.622	3700 - 4300	3700 - 4500	3500 - 4300	3500 - 4500	3300 - 4500	3100 - 4500	3100 - 4500	3100 - 4500
16538.583	-3.115	3.438	3700 - 4300	3700 - 4300	3500 - 4300	3500 - 4500	3300 - 4500	3300 - 4300	3300 - 4300	3300 - 4300
16729.779	-2.788	2.346	3700 - 4100	3700 - 4300	3500 - 4300	3300 - 4300	3300 - 4300	3100 - 4300	3100 - 4100	3100 - 4100
16866.688	-2.988	3.852	3700 - 4300	3700 - 4300	3500 - 4300	3500 - 4300	3300 - 4300	3100 - 4300	3300 - 4300	3100 - 4300
16879.082	-3.069	4.061	3700 - 4300	3700 - 4300	3500 - 4300	3500 - 4300	3300 - 4300	3300 - 4300	3100 - 4300	3300 - 4300
16886.269	-2.116	11.34	3900 - 4300	3700 - 4100	3500 - 4300	3500 - 3900	3300 - 4300	3100 - 4100	3100 - 4100	3100 - 4100
16895.179	-2.907	12.31	3700 - 4300	3700 - 4500	3500 - 4300	3500 - 4300	3100 - 4500	3500 - 4500	3300 - 4300	3300 - 4300
16898.766	-2.978	20.83	3700 - 4300	3700 - 4500	3500 - 4300	3300 - 4500	3100 - 4300	3300 - 4300	3100 - 4300	3100 - 4500
16902.728	-2.606	11.14	3700 - 4100	3700 - 4500	3500 - 4300	3300 - 4300	3500 - 4300	3100 - 4300	3300 - 4300	3300 - 3900
16904.275	-2.781	10.00	3700 - 4500	3700 - 4300	3700 - 4300	3300 - 4100	3100 - 4300	3100 - 4300	3300 - 4300	3100 - 3900
16909.284	-2.693	5.786	3700 - 4100	3700 - 4500	3500 - 4300	3500 - 4300	3500 - 4300	3500 - 4300	3300 - 4300	3500 - 4300

Table 4.2: OH-lines 16052.765Å to 16909.284Å with average scatter bigger than 0.03. See table **??** for a detailed organisation of this table. See table 3.1 for a detailed organisation of this table

Appendix B

Here, all 68 OH-lines with data split into metallicity bins are presented one after the other. The subplots follow the same metallicity as in figures 3.5 and 3.6:

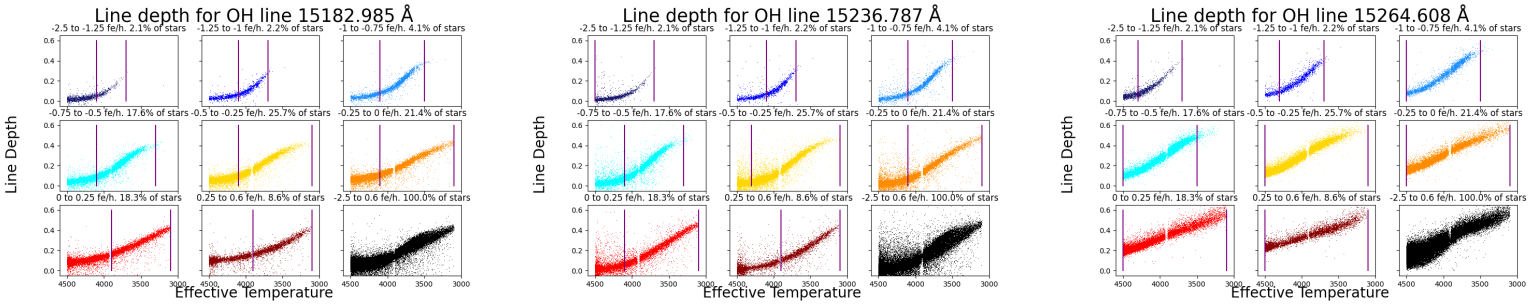
Line depth for OH line 15182.985 Å
Line depth for OH line 15236.787 Å
Line depth for OH line 15264.608 Å
Line depth for OH line 15266.172 Å
Line depth for OH line 15278.528 Å
Line depth for OH line 15281.057 Å
Line depth for OH line 15391.126 Å
Line depth for OH line 15407.292 Å
Line depth for OH line 15409.178 Å
Line depth for OH line 15419.464 Å
Line depth for OH line 15422.371 Å
Line depth for OH line 15427.48 Å
Line depth for OH line 15428.397 Å
Line depth for OH line 15505.53 Å
Line depth for OH line 15535.461 Å
Line depth for OH line 15560.248 Å
Line depth for OH line 15568.785 Å
Line depth for OH line 15572.088 Å
-2.5 to -1.25 fe/h. 2.1% of stars
-1.25 to -1 fe/h. 2.2% of stars
-1 to -0.75 fe/h. 4.1% of stars
-0.75 to -0.5 fe/h. 17.6% of stars
-0.5 to -0.25 fe/h. 25.7% of stars
-0.25 to 0 fe/h. 21.4% of stars
0 to 0.25 fe/h. 18.3% of stars
0.25 to 0.6 fe/h. 8.6% of stars
-2.5 to 0.6 fe/h. 100.0% of stars
Line Depth
Effective Temperature

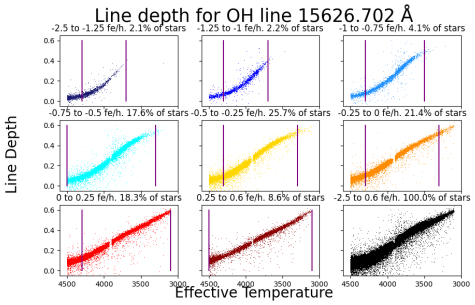
Line depth for OH line 15626.702 Å
-2.5 to -1.25 fe/h. 2.1% of stars
-1.25 to -1 fe/h. 2.2% of stars
-1 to -0.75 fe/h. 4.1% of stars
-0.75 to -0.5 fe/h. 17.6% of stars
-0.5 to -0.25 fe/h. 25.7% of stars
-0.25 to 0 fe/h. 21.4% of stars
0 to 0.25 fe/h. 18.3% of stars
0.25 to 0.6 fe/h. 8.6% of stars
-2.5 to 0.6 fe/h. 100.0% of stars
Line Depth
Effective Temperature

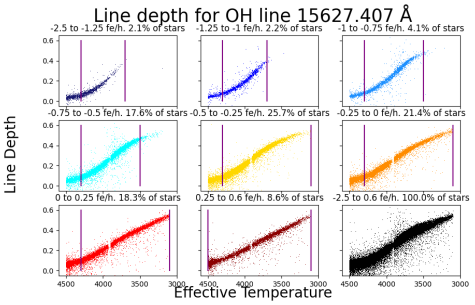
Line depth for OH line 15627.407 Å
-2.5 to -1.25 fe/h. 2.1% of stars
-1.25 to -1 fe/h. 2.2% of stars
-1 to -0.75 fe/h. 4.1% of stars
-0.75 to -0.5 fe/h. 17.6% of stars
-0.5 to -0.25 fe/h. 25.7% of stars
-0.25 to 0 fe/h. 21.4% of stars
0 to 0.25 fe/h. 18.3% of stars
0.25 to 0.6 fe/h. 8.6% of stars
-2.5 to 0.6 fe/h. 100.0% of stars
Line Depth
Effective Temperature

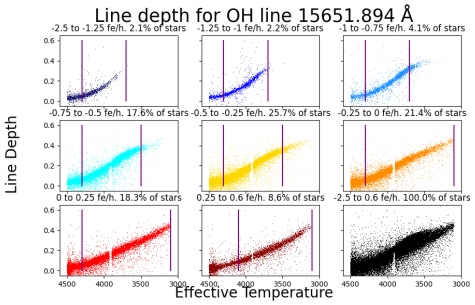
Line depth for OH line 15651.894 Å
-2.5 to -1.25 fe/h. 2.1% of stars
-1.25 to -1 fe/h. 2.2% of stars
-1 to -0.75 fe/h. 4.1% of stars
-0.75 to -0.5 fe/h. 17.6% of stars
-0.5 to -0.25 fe/h. 25.7% of stars
-0.25 to 0 fe/h. 21.4% of stars
0 to 0.25 fe/h. 18.3% of stars
0.25 to 0.6 fe/h. 8.6% of stars
-2.5 to 0.6 fe/h. 100.0% of stars
Line Depth
Effective Temperature

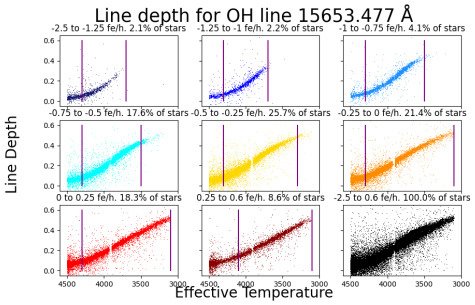
Line depth for OH line 15653.477 Å
-2.5 to -1.25 fe/h. 2.1% of stars
-1.25 to -1 fe/h. 2.2% of stars
-1 to -0.75 fe/h. 4.1% of stars
-0.75 to -0.5 fe/h. 17.6% of stars
-0.5 to -0.25 fe/h. 25.7% of stars
-0.25 to 0 fe/h. 21.4% of stars
0 to 0.25 fe/h. 18.3% of stars
0.25 to 0.6 fe/h. 8.6% of stars
-2.5 to 0.6 fe/h. 100.0% of stars
Line Depth
Effective Temperature

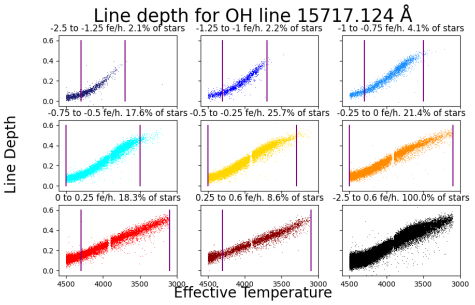
Line depth for OH line 15717.124 Å
-2.5 to -1.25 fe/h. 2.1% of stars
-1.25 to -1 fe/h. 2.2% of stars
-1 to -0.75 fe/h. 4.1% of stars
-0.75 to -0.5 fe/h. 17.6% of stars
-0.5 to -0.25 fe/h. 25.7% of stars
-0.25 to 0 fe/h. 21.4% of stars
0 to 0.25 fe/h. 18.3% of stars
0.25 to 0.6 fe/h. 8.6% of stars
-2.5 to 0.6 fe/h. 100.0% of stars
Line Depth
Effective Temperature

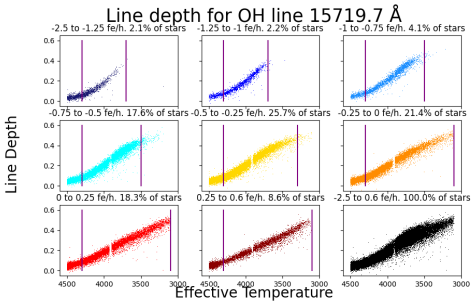
Line depth for OH line 15719.7 Å
-2.5 to -1.25 fe/h. 2.1% of stars
-1.25 to -1 fe/h. 2.2% of stars
-1 to -0.75 fe/h. 4.1% of stars
-0.75 to -0.5 fe/h. 17.6% of stars
-0.5 to -0.25 fe/h. 25.7% of stars
-0.25 to 0 fe/h. 21.4% of stars
0 to 0.25 fe/h. 18.3% of stars
0.25 to 0.6 fe/h. 8.6% of stars
-2.5 to 0.6 fe/h. 100.0% of stars
Line Depth
Effective Temperature

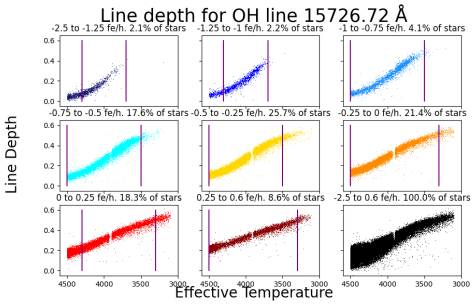
Line depth for OH line 15726.72 Å
-2.5 to -1.25 fe/h. 2.1% of stars
-1.25 to -1 fe/h. 2.2% of stars
-1 to -0.75 fe/h. 4.1% of stars
-0.75 to -0.5 fe/h. 17.6% of stars
-0.5 to -0.25 fe/h. 25.7% of stars
-0.25 to 0 fe/h. 21.4% of stars
0 to 0.25 fe/h. 18.3% of stars
0.25 to 0.6 fe/h. 8.6% of stars
-2.5 to 0.6 fe/h. 100.0% of stars
Line Depth
Effective Temperature

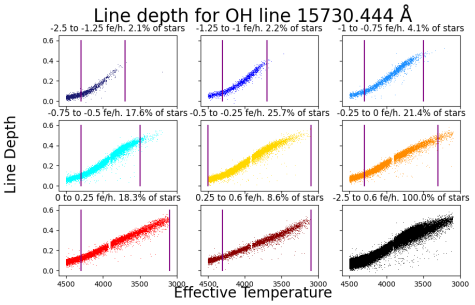
Line depth for OH line 15730.444 Å
-2.5 to -1.25 fe/h. 2.1% of stars
-1.25 to -1 fe/h. 2.2% of stars
-1 to -0.75 fe/h. 4.1% of stars
-0.75 to -0.5 fe/h. 17.6% of stars
-0.5 to -0.25 fe/h. 25.7% of stars
-0.25 to 0 fe/h. 21.4% of stars
0 to 0.25 fe/h. 18.3% of stars
0.25 to 0.6 fe/h. 8.6% of stars
-2.5 to 0.6 fe/h. 100.0% of stars
Line Depth
Effective Temperature

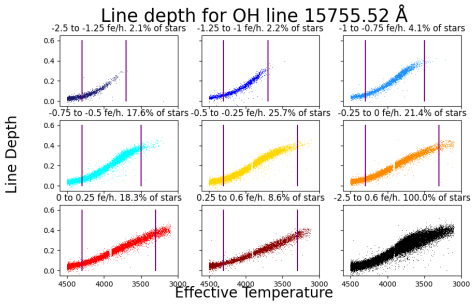
Line depth for OH line 15755.52 Å
-2.5 to -1.25 fe/h. 2.1% of stars
-1.25 to -1 fe/h. 2.2% of stars
-1 to -0.75 fe/h. 4.1% of stars
-0.75 to -0.5 fe/h. 17.6% of stars
-0.5 to -0.25 fe/h. 25.7% of stars
-0.25 to 0 fe/h. 21.4% of stars
0 to 0.25 fe/h. 18.3% of stars
0.25 to 0.6 fe/h. 8.6% of stars
-2.5 to 0.6 fe/h. 100.0% of stars
Line Depth
Effective Temperature

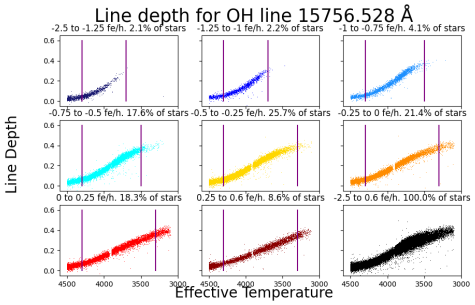
Line depth for OH line 15756.528 Å
-2.5 to -1.25 fe/h. 2.1% of stars
-1.25 to -1 fe/h. 2.2% of stars
-1 to -0.75 fe/h. 4.1% of stars
-0.75 to -0.5 fe/h. 17.6% of stars
-0.5 to -0.25 fe/h. 25.7% of stars
-0.25 to 0 fe/h. 21.4% of stars
0 to 0.25 fe/h. 18.3% of stars
0.25 to 0.6 fe/h. 8.6% of stars
-2.5 to 0.6 fe/h. 100.0% of stars
Line Depth
Effective Temperature

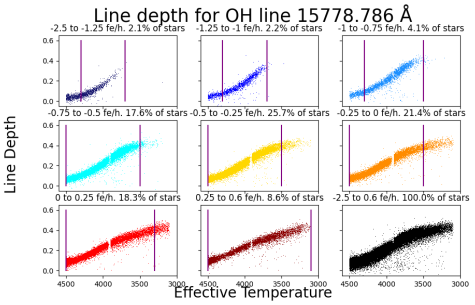
Line depth for OH line 15778.786 Å
-2.5 to -1.25 fe/h. 2.1% of stars
-1.25 to -1 fe/h. 2.2% of stars
-1 to -0.75 fe/h. 4.1% of stars
-0.75 to -0.5 fe/h. 17.6% of stars
-0.5 to -0.25 fe/h. 25.7% of stars
-0.25 to 0 fe/h. 21.4% of stars
0 to 0.25 fe/h. 18.3% of stars
0.25 to 0.6 fe/h. 8.6% of stars
-2.5 to 0.6 fe/h. 100.0% of stars
Line Depth
Effective Temperature

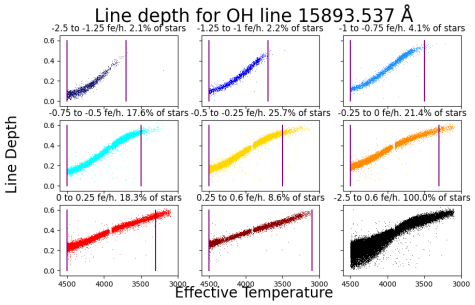
Line depth for OH line 15893.537 Å
-2.5 to -1.25 fe/h. 2.1% of stars
-1.25 to -1 fe/h. 2.2% of stars
-1 to -0.75 fe/h. 4.1% of stars
-0.75 to -0.5 fe/h. 17.6% of stars
-0.5 to -0.25 fe/h. 25.7% of stars
-0.25 to 0 fe/h. 21.4% of stars
0 to 0.25 fe/h. 18.3% of stars
0.25 to 0.6 fe/h. 8.6% of stars
-2.5 to 0.6 fe/h. 100.0% of stars
Line Depth
Effective Temperature

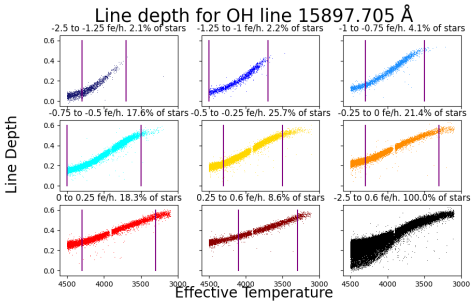
Line depth for OH line 15897.705 Å
-2.5 to -1.25 fe/h. 2.1% of stars
-1.25 to -1 fe/h. 2.2% of stars
-1 to -0.75 fe/h. 4.1% of stars
-0.75 to -0.5 fe/h. 17.6% of stars
-0.5 to -0.25 fe/h. 25.7% of stars
-0.25 to 0 fe/h. 21.4% of stars
0 to 0.25 fe/h. 18.3% of stars
0.25 to 0.6 fe/h. 8.6% of stars
-2.5 to 0.6 fe/h. 100.0% of stars
Line Depth
Effective Temperature

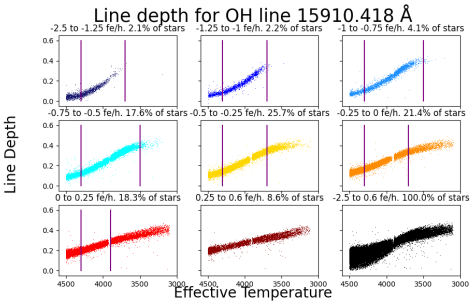
Line depth for OH line 15910.418 Å
-2.5 to -1.25 fe/h. 2.1% of stars
-1.25 to -1 fe/h. 2.2% of stars
-1 to -0.75 fe/h. 4.1% of stars
-0.75 to -0.5 fe/h. 17.6% of stars
-0.5 to -0.25 fe/h. 25.7% of stars
-0.25 to 0 fe/h. 21.4% of stars
0 to 0.25 fe/h. 18.3% of stars
0.25 to 0.6 fe/h. 8.6% of stars
-2.5 to 0.6 fe/h. 100.0% of stars
Line Depth
Effective Temperature

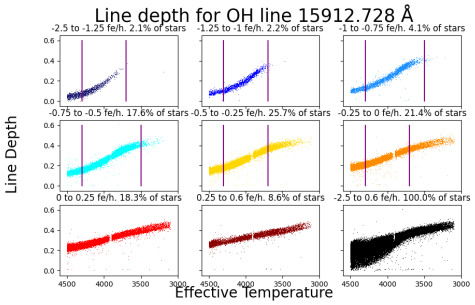
Line depth for OH line 15912.728 Å
-2.5 to -1.25 fe/h. 2.1% of stars
-1.25 to -1 fe/h. 2.2% of stars
-1 to -0.75 fe/h. 4.1% of stars
-0.75 to -0.5 fe/h. 17.6% of stars
-0.5 to -0.25 fe/h. 25.7% of stars
-0.25 to 0 fe/h. 21.4% of stars
0 to 0.25 fe/h. 18.3% of stars
0.25 to 0.6 fe/h. 8.6% of stars
-2.5 to 0.6 fe/h. 100.0% of stars
Line Depth
Effective Temperature

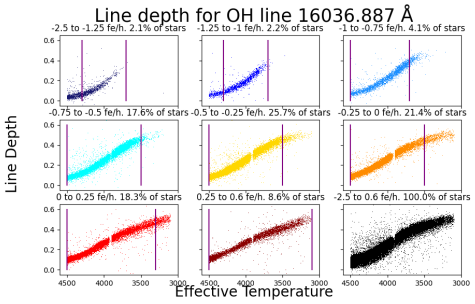
Line depth for OH line 16036.887 Å
-2.5 to -1.25 fe/h. 2.1% of stars
-1.25 to -1 fe/h. 2.2% of stars
-1 to -0.75 fe/h. 4.1% of stars
-0.75 to -0.5 fe/h. 17.6% of stars
-0.5 to -0.25 fe/h. 25.7% of stars
-0.25 to 0 fe/h. 21.4% of stars
0 to 0.25 fe/h. 18.3% of stars
0.25 to 0.6 fe/h. 8.6% of stars
-2.5 to 0.6 fe/h. 100.0% of stars
Line Depth
Effective Temperature

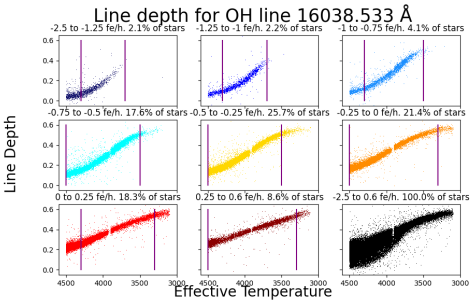
Line depth for OH line 16038.533 Å
-2.5 to -1.25 fe/h. 2.1% of stars
-1.25 to -1 fe/h. 2.2% of stars
-1 to -0.75 fe/h. 4.1% of stars
-0.75 to -0.5 fe/h. 17.6% of stars
-0.5 to -0.25 fe/h. 25.7% of stars
-0.25 to 0 fe/h. 21.4% of stars
0 to 0.25 fe/h. 18.3% of stars
0.25 to 0.6 fe/h. 8.6% of stars
-2.5 to 0.6 fe/h. 100.0% of stars
Line Depth
Effective Temperature

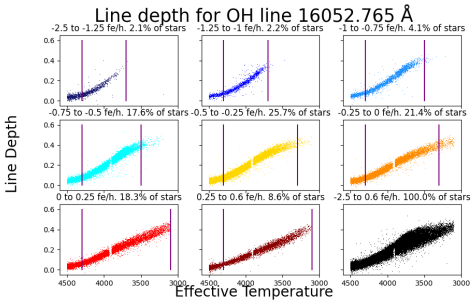
Line depth for OH line 16052.765 Å
-2.5 to -1.25 fe/h. 2.1% of stars
-1.25 to -1 fe/h. 2.2% of stars
-1 to -0.75 fe/h. 4.1% of stars
-0.75 to -0.5 fe/h. 17.6% of stars
-0.5 to -0.25 fe/h. 25.7% of stars
-0.25 to 0 fe/h. 21.4% of stars
0 to 0.25 fe/h. 18.3% of stars
0.25 to 0.6 fe/h. 8.6% of stars
-2.5 to 0.6 fe/h. 100.0% of stars
Line Depth
Effective Temperature

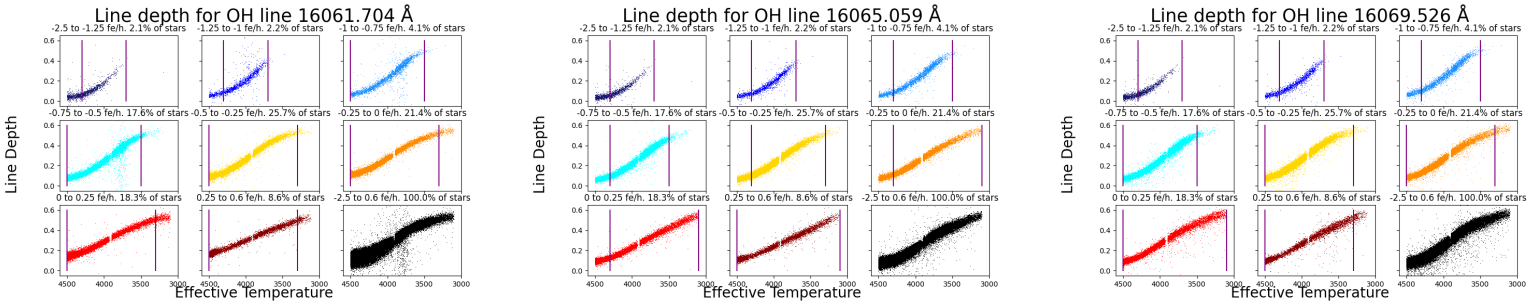
Line depth for OH line 16061.704 Å
Line depth for OH line 16065.059 Å
Line depth for OH line 16069.526 Å
-2.5 to -1.25 fe/h. 2.1% of stars
-1.25 to -1 fe/h. 2.2% of stars
-1 to -0.75 fe/h. 4.1% of stars
-0.75 to -0.5 fe/h. 17.6% of stars
-0.5 to -0.25 fe/h. 25.7% of stars
-0.25 to 0 fe/h. 21.4% of stars
0 to 0.25 fe/h. 18.3% of stars
0.25 to 0.6 fe/h. 8.6% of stars
-2.5 to 0.6 fe/h. 100.0% of stars
Line Depth
Effective Temperature

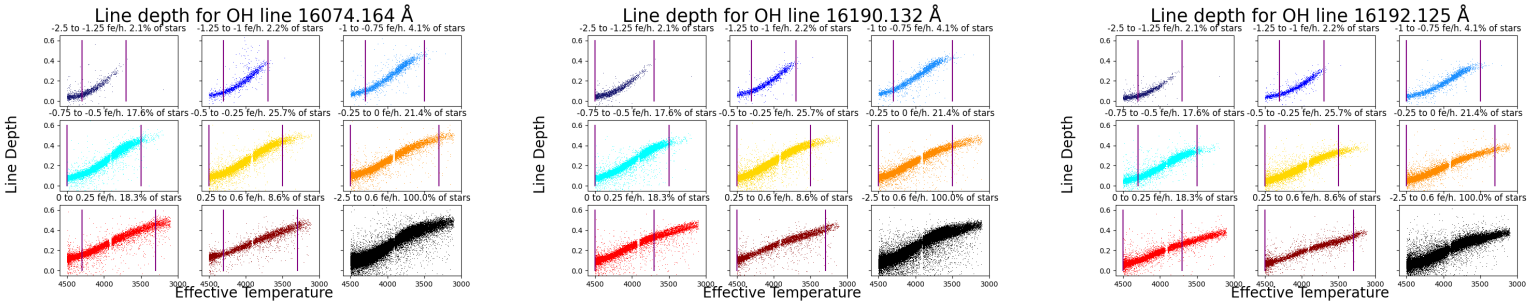
Line depth for OH line 16074.164 Å
Line depth for OH line 16190.132 Å
Line depth for OH line 16192.125 Å
-2.5 to -1.25 fe/h. 2.1% of stars
-1.25 to -1 fe/h. 2.2% of stars
-1 to -0.75 fe/h. 4.1% of stars
-0.75 to -0.5 fe/h. 17.6% of stars
-0.5 to -0.25 fe/h. 25.7% of stars
-0.25 to 0 fe/h. 21.4% of stars
0 to 0.25 fe/h. 18.3% of stars
0.25 to 0.6 fe/h. 8.6% of stars
-2.5 to 0.6 fe/h. 100.0% of stars
Line Depth
Effective Temperature

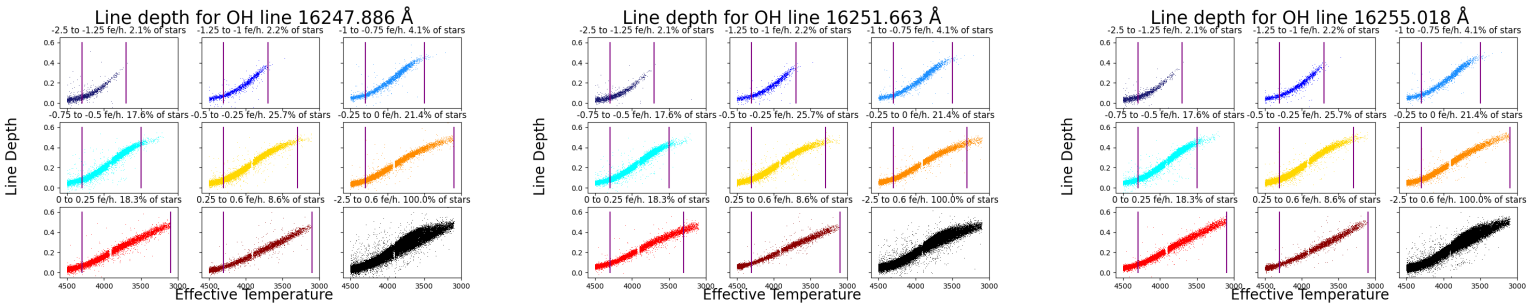
Line depth for OH line 16247.886 Å
Line depth for OH line 16251.663 Å
Line depth for OH line 16255.018 Å
-2.5 to -1.25 fe/h. 2.1% of stars
-1.25 to -1 fe/h. 2.2% of stars
-1 to -0.75 fe/h. 4.1% of stars
-0.75 to -0.5 fe/h. 17.6% of stars
-0.5 to -0.25 fe/h. 25.7% of stars
-0.25 to 0 fe/h. 21.4% of stars
0 to 0.25 fe/h. 18.3% of stars
0.25 to 0.6 fe/h. 8.6% of stars
-2.5 to 0.6 fe/h. 100.0% of stars
Line Depth
Effective Temperature

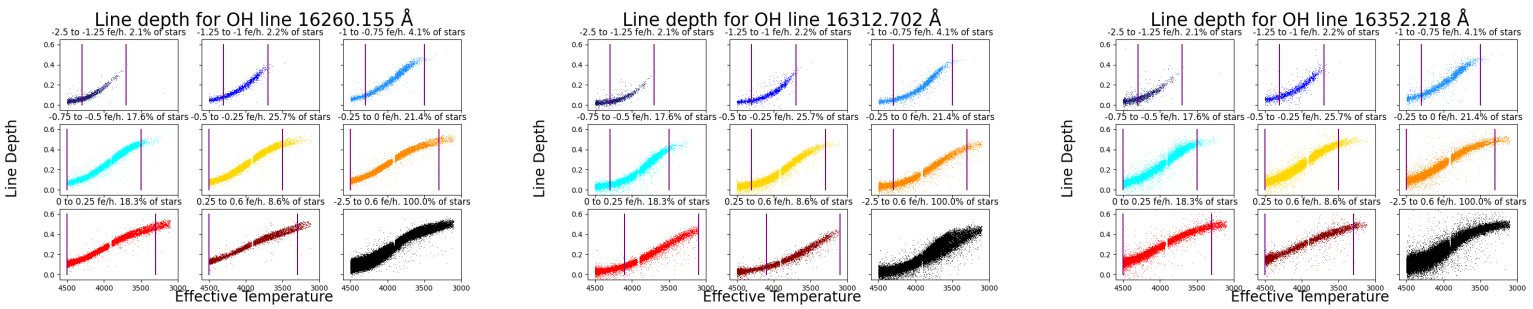
Line depth for OH line 16260.155 Å
Line depth for OH line 16312.702 Å
Line depth for OH line 16352.218 Å
-2.5 to -1.25 fe/h. 2.1% of stars
-1.25 to -1 fe/h. 2.2% of stars
-1 to -0.75 fe/h. 4.1% of stars
-0.75 to -0.5 fe/h. 17.6% of stars
-0.5 to -0.25 fe/h. 25.7% of stars
-0.25 to 0 fe/h. 21.4% of stars
0 to 0.25 fe/h. 18.3% of stars
0.25 to 0.6 fe/h. 8.6% of stars
-2.5 to 0.6 fe/h. 100.0% of stars
Line Depth
Effective Temperature

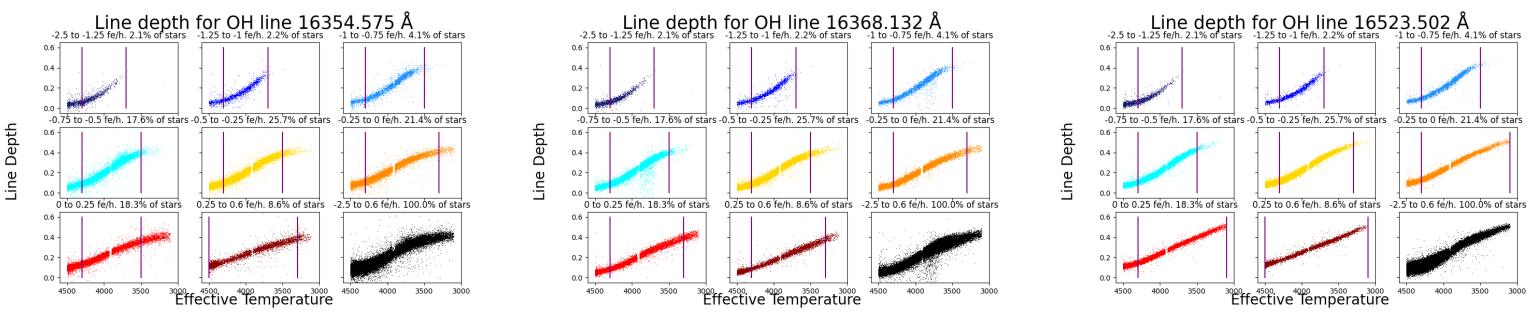
Line depth for OH line 16354.575 Å
Line depth for OH line 16368.132 Å
Line depth for OH line 16523.502 Å
-2.5 to -1.25 fe/h. 2.1% of stars
-1.25 to -1 fe/h. 2.2% of stars
-1 to -0.75 fe/h. 4.1% of stars
-0.75 to -0.5 fe/h. 17.6% of stars
-0.5 to -0.25 fe/h. 25.7% of stars
-0.25 to 0 fe/h. 21.4% of stars
0 to 0.25 fe/h. 18.3% of stars
0.25 to 0.6 fe/h. 8.6% of stars
-2.5 to 0.6 fe/h. 100.0% of stars
Line Depth
Effective Temperature

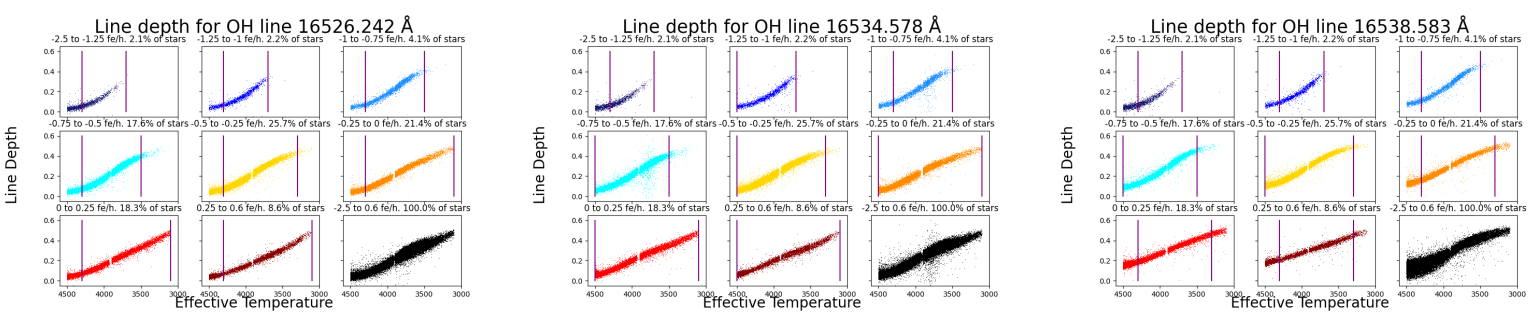
Line depth for OH line 16526.242 Å
Line depth for OH line 16534.578 Å
Line depth for OH line 16538.583 Å
-2.5 to -1.25 fe/h. 2.1% of stars
-1.25 to -1 fe/h. 2.2% of stars
-1 to -0.75 fe/h. 4.1% of stars
-0.75 to -0.5 fe/h. 17.6% of stars
-0.5 to -0.25 fe/h. 25.7% of stars
-0.25 to 0 fe/h. 21.4% of stars
0 to 0.25 fe/h. 18.3% of stars
0.25 to 0.6 fe/h. 8.6% of stars
-2.5 to 0.6 fe/h. 100.0% of stars
Line Depth
Effective Temperature

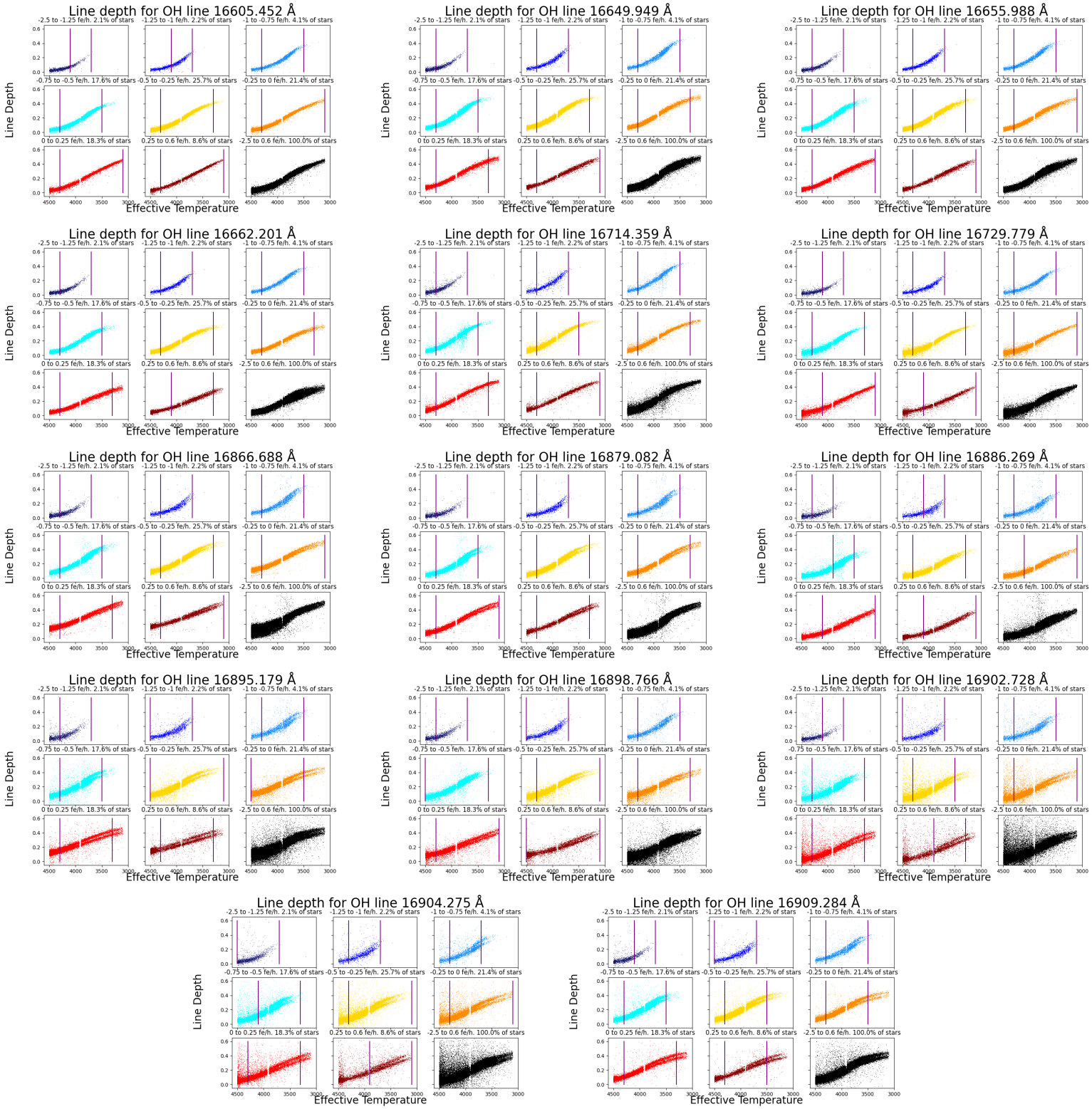

Figure 4.1: 86 temperature sensitive OH-lines. See figure 3.5 for a detailed summery of how to read each plot.